

Adsorption and Inhibition Mechanisms of New Pyrazole Derivatives for Carbon Steel Corrosion in Hydrochloric Acid Solutions Based on Experimental, Computational, and Theoretical Calculations

Loubna Adlani, Nisrine Benzbiria, Abderrahim Titi, Nadia Timoudan, Ismail Warad, Abeer AlObaid, Basheer Mohammed Al-Maswari, Fouad Benhiba,* Rachid Touzani, Hassan Zarrok, Fouad Bentiss, Hassan Oudda, and Abdelkader Zarrouk*

Cite This: *ACS Omega* 2024, 9, 13746–13763

Read Online

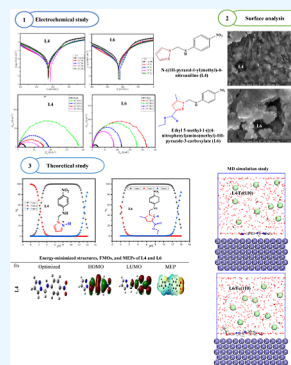
ACCESS |

Metrics & More

Article Recommendations

Supporting Information

ABSTRACT: The study aims to synthesize two green pyrazole compounds, *N*-((1*H*-pyrazol-1-yl)methyl)-4-nitroaniline (L4) and ethyl 5-methyl-1-(((4-nitrophenyl)amino)methyl)-1*H*-pyrazole-3-carboxylate (L6), and test their action as corrosion inhibitors for carbon steel (CS) in a 1 M HCl solution. Both chemical and electrochemical methods, namely, gravimetric measurements (WL), potentiodynamic polarization (PDP), and electrochemical impedance spectroscopy (EIS), were used to assess the efficiency of the investigated molecules. DFT calculations at B3LYP/6-31++G (d, p) and molecular dynamics simulation were used to carry out quantum chemical calculations in order to link their electronic characteristics with the findings of experiments. The organic products exhibited good anticorrosion ability, with maximum inhibition efficiencies (IE %) of 91.8 and 90.8% for 10⁻³ M L6 and L4, respectively. In accordance with PDP outcomes, L6 and L4 inhibitors act as mixed-type inhibitors. Assessment of the temperature influence evinces that both L4 and L6 are chemisorbed on CS. The adsorption of L4 and L6 on CS appears to follow the Langmuir isotherm. Scanning electron microscopy and UV–visible disclose the constitution of a barrier layer, limiting the accessibility of corrosive species to the CS surface. Theoretical studies were performed to support the results derived from experimental techniques (WL, PDP, and EIS).



1. INTRODUCTION

As a universal issue, corrosion leads to tremendous safety and economic casualties worldwide.^{1–3} Beyond that, corrosion also gives rise to environmental hazards as a result of the release of poisonous solvents and chemicals via the corrosion-ridden metallic components.^{4,5} Carbon steel (CS) and other iron alloys are commonly employed in various industrial processes, some of which involve the employment of overly concentrated acids.^{6,7} As a result, a significant portion of metallic components are lost owing to corrosion.^{8–10} Given the massive losses, a variety of corrosion prevention approaches have been devised to suit the budget, the nature of the metal, and the media.^{11–13} Regardless, the most prevalent and frequently used method is the application of organic products as inhibitors since they are efficient, easily synthesized, and show high inhibition performance coupled to cost effectiveness. In most cases, the mitigation of corrosion is achieved by developing a protective layer at the interface metal/medium.^{14–23} According to the literature, electron-rich centers as polar functional groups (–NO₂, –NH₂, –NHMe, –OH, –OMe, –CN, etc.) and double/triple links (>C=O, –N=O, –C≡C–, –C≡N, >C=S, –N=N–, etc.) of the aromatic ring (s) and/or side chain are considered as good adsorption centers.^{24–26} While a number of heterocycles were assessed as

potent inhibitors, the main focus of current investigations is on developing cost-effective and eco-friendly compounds. Pyrazole derivatives constitute one such alternative as they are heterocyclic products used in several fields, nontoxic (used as dyes, pesticides, insecticides, fungicides, and herbicides), and relevant candidates to mitigate the corrosion of metals. Some of the research conducted on the prohibition activity of pyrazole derivatives against CS corrosion in 1 M HCl is reported in [Table 1](#).^{22–25}

In the current investigation, the inhibitory capacity of two novel pyrazole compounds, namely, *N*-((1*H*-pyrazol-1-yl)methyl)-4-nitroaniline (L4) and ethyl 5-methyl-1-(((4-nitrophenyl)amino)methyl)-1*H*-pyrazole-3-carboxylate (L6), was investigated against the degradation of CS in molar HCl medium. The innovative aspect of our work lies in the fact that the selected compounds are employed for the first time as corrosion inhibitors. In addition, pyrazole derivatives have a

Received: October 21, 2023

Revised: February 12, 2024

Accepted: February 20, 2024

Published: March 5, 2024

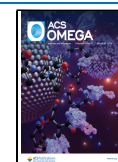
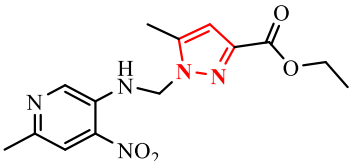
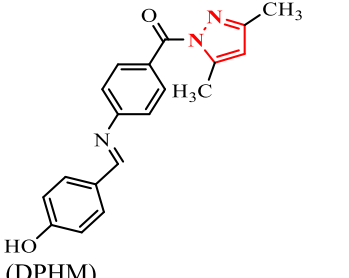
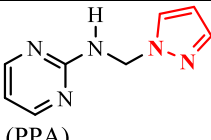
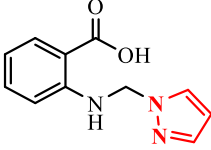
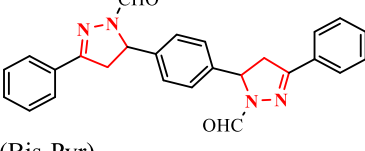
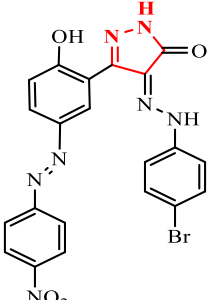


Table 1. Inhibition Efficiencies of Some Tested Pyrazole Products as Corrosion Inhibitors of CS in 1 M HCl Medium

Pyrazole derivative	Inhibition efficiency	Concentration	Temperature	Ref.
	92%	10^{-3} M	303K	²⁷
 (EMPC)				
 (DPHM)	89.5%	400 ppm	333 K	²⁸
 (PPA)	94%	10^{-3} M	303 K	²⁹
 (PMB)	92%	10^{-3} M	303 K	²⁹
 (Bis-Pyr)	91%	400 ppm	298 K	³⁰
	93.6%	500ppm	298K	³¹

variety of substituents; therefore, the outcomes of this work would be useful for researchers to devise, improve, and synthesize further efficient corrosion inhibitors.

A variety of both electrochemical and chemical methods were employed for this purpose. The morphology and nature of the protecting film developed on CS were inspected by using scanning electron microscopy (SEM). The UV–visible analysis was executed to gain insight into L4 and L6 inhibitor adsorption on the metallic surface. Outputs of theoretical investigations were examined and discussed to support the experimental results.

2. EXPERIMENTAL METHODS

2.1. Materials. The material used to conduct this study is a CS bar with the following elemental compositions (wt %): C (0.370), Si (0.230), Mn (0.680), Cr (0.077), S (0.016), Ti (0.011), Ni (0.059), Co (0.059), Cu (0.16), and Fe (remainder). Before each experiment, the surface of the metal was polished mechanically in freshwater using sand paper with progressively finer particle sizes ranging from 180 to 1200. Then, the samples were washed with distilled water, degreased with acetone, and air-dried.

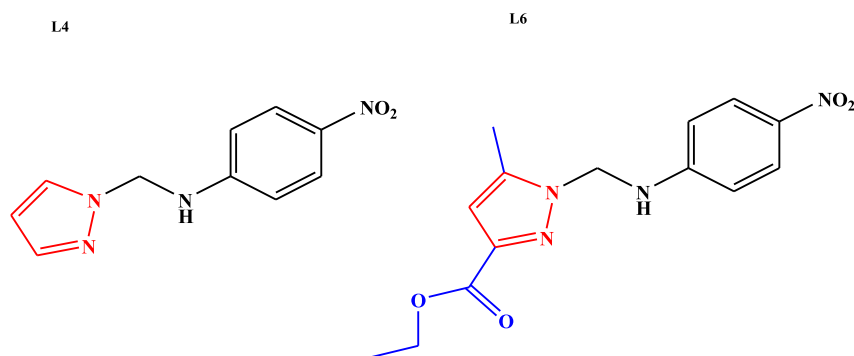


Figure 1. *N*-((1*H*-Pyrazol-1-yl)methyl)-4-nitroaniline (L4) and ethyl 5-methyl-1-(((4-nitrophenyl)amino)methyl)-1*H*-pyrazole-3-carboxylate (L6).

2.2. Chemicals. All of the chemicals provided by Sigma-Aldrich were used without additional modification. Figure 1 depicts the architecture of L4 and L6.

Analytical commercial-grade 37% HCl was diluted with twice-distilled water to create molar HCl aqueous solutions. The L4 and L6 inhibitor doses used for the corrosion trials ranged from 10^{-3} to 10^{-6} M in a 1 M HCl solution devoid of the inhibitors. The electrochemical tests were carried out in a room with regular air and no turbulence. It is to be highlighted that L6 exhibits stability in hydrolysis due to its aromatic ester nature. Additionally, the ester function strongly interacts with the pyrazole through a conjugated system. This conjugation further reinforces the molecular structure, providing additional protection against hydrolysis. Thus, the combination of aromatic esterification and the conjugated system imparts an enhanced resistance to the hydrolysis reaction.

2.3. Electrochemical Apparatus and Measurements. A standard three-electrode cell is used, consisting of a CS working electrode (WE), a wire of Pt acting as the counter electrode, and a saturated calomel electrode (SCE) acting as the reference electrode. The electrochemical cell, which contained 100 mL of diluted hydrochloric acid, completely submerged the electrodes. With the exception of the impact temperature research, all studies were carried out at room temperature without stirring.

Data on electrochemistry [electrochemical impedance spectroscopy (EIS) and potentiodynamic polarization (PDP)] was gathered using a potentiostat made by Volta Lab (PGZ 100) and VoltaMaster software. The generated curves were used to investigate how well CS corroded in molar HCl in the absence of L4 or L6 and in its presence.

The WE was kept submerged in the electrolyte for 30 min in order to establish a steady open-circuit potential (E_{OCP}). The electrochemical tests were then conducted. The polarization graphs were plotted at a rate of 5×10^{-4} V/s, scanning from -0.8 to 0 V/SCE. The linear polarization resistance was measured by drawing the electrode potential ± 0.01 V vs E_{OCP} starting at a greater negative potential. Prior to all testing, the voltage had been stable for more than 30 min.

The electrochemical measurements were triple-realized for each inhibitor concentration to ensure reproducibility.

The inhibitory efficiency was calculated using the following formula

$$\text{IE}_{\text{POL}}(\%) = \frac{i_{\text{corr}} - i_{\text{corr}}(\text{inhib})}{i_{\text{corr}}} \times 100 \quad (1)$$

The corrosion current densities in the presence and absence of chemical inhibitors are thus represented by the symbols i_{corr} and $i_{\text{corr}}(\text{inhib})$.

The EIS measurements were drawn at E_{OCP} using the same workstation as before, utilizing an AC signal with an amplitude of 10 mV and a frequency domain of 10^5 to 10^{-2} Hz. ZView software, version 3.4, used the Nyquist model to analyze the EIS charts for a selected equivalent electrical circuit.

The inhibitory efficacy utilizing EIS was calculated using the formula shown in ref 31

$$\text{IE}_{\text{EIS}}(\%) = \frac{R_p(\text{inhib}) - R_p}{R_p(\text{inhib})} \times 100 \quad (2)$$

The values of polarization resistance in the presence and absence of the inhibitor are indicated by the symbols $R_p(\text{inhib})$ and R_p .

Since we operated in the same settings, we were able to use the results that had already been published by our team for the effects of temperature and concentration using stationary and transient polarization techniques in the absence of an inhibitor.³²

2.4. Gravimetric Measurements. The NACE/ASTM 169/G31–12a: Standard Guide for Laboratory Immersion Corrosion Testing of Metals³³ was followed in handling the WL trials of CS in the test medium. The test medium contained 100 mL of 1 M HCl at 303 K together with L4 or L6 at various concentrations (10^{-6} , 10^{-5} , 10^{-4} , and 10^{-3} M). The CS panels ($2.0 \times 2.0 \times 0.1$ cm) were mechanically polished using sand papers with grade nos 400, 600, 800, 1000, and 1200 to achieve a mirror finish. They were then successively cleaned with deionized water and anhydrous ethanol. The CS panels were immersed in the test liquid at 303 K for 6 h after their masses were precisely weighed and recorded. In order to remove the corrosive compounds that had accumulated on the CS surface, the CS panels were then disassembled and cleaned with deionized water. After being dried by cool air, the cleaned CS panels were weighed once more to determine their exact masses after corrosion. Equation 3 was used to calculate the inhibition efficiencies (IE_{WL}) of L4 and L6 for CS in the test medium³⁴

$$\text{IE}_{\text{WL}}(\%) = \frac{C_R^0 - C_R}{C_R^0} \times 100 \quad (3)$$

where C_R^0 and C_R stand for the weight loss of the CS panel in the test media without and with the inhibitory drug present, respectively.

The operating temperature for the temperature effect component was gradually increased from 303 to 333 K in a solution containing 10^{-3} M L4 or L6 inhibitors.

2.5. UV–Vis Study. The efficiency of the inhibitor against corrosion was examined using the absorption UV–visible spectroscopy method. It is based on how well they can absorb light of particular wavelengths. Measurements of solution absorbance were made with and without the presence of the C-steel sample for 72 h in the acidic medium at 10^{-3} M L4 or L6, in order to investigate how organic molecules interact with the metallic substrate in the molar HCl medium. Between 200 and 600 nm wavelengths were scanned. It has been done using a JASCO V-700 UV–visible spectrophotometer.

2.6. SEM Explorations. Surface examinations were conducted using the SEM method. It was decided upon the ideal concentration of 10^{-3} M corrosive solutions, both with and without inhibiting molecules. The samples were individually subjected to the aforementioned aggressive media for 24 h before being gently removed, rinsed with purified water, dried, and assessed for surface morphological examination by SEM. The surface morphology was investigated using the JEOL-JSM-IT-100 model. SEM images taken at 10,000 \times magnification showed the metal in question. Since we carried out the experiments under the same conditions, we were able to use the results already published by our team for the SEM–EDX analysis.³⁵

2.7. DFT and MD Details. We made an effort to look into the mechanism of action of the pyrazole analogues on the Fe surface using the DFT technique in the aqueous phase.³⁶ This theoretical innovation was also made to link chemical reactivity indices to the estimated experimental inhibitory efficacy of neutral and protonated pyrazole analogues.³⁷ The molecular structure of the molecules under examination was optimized using the Gauss. 09 software program to the final geometry at the DFT/B3LYP/6-31++G (d, p).³⁸ E_{LUMO} , E_{HOMO} , ΔE , global electronegativity $\langle\langle\chi\rangle\rangle$, global hardness $\langle\langle\eta\rangle\rangle$, and electrons transferred $\langle\langle\Delta N_{110}\rangle\rangle$ from occupied organic molecule orbitals to vacant orbitals of metal surface. With $\Phi = \chi(\text{Fe110}) = 4.82$ eV, the work function (eq 7) explains the theoretical value of χ in Fe(110).³⁹

$$\Delta E = E_{\text{LUMO}} - E_{\text{HOMO}} \quad (4)$$

$$\chi = \frac{1}{2}(E_{\text{HOMO}} + E_{\text{LUMO}}) \quad (5)$$

$$\eta = \frac{1}{2}(E_{\text{HOMO}} - E_{\text{LUMO}}) \quad (6)$$

$$\Delta N_{110} = \frac{\chi_{\text{Fe110}} - \chi_{\text{inh}}}{2(\eta_{\text{Fe110}} + \eta_{\text{inh}})} = \frac{\Phi - \chi_{\text{inh}}}{2\eta_{\text{inh}}} \quad (7)$$

Investigations of the interactions of molecules investigated with Fe(110) systems are done using MD simulations. This simulation was carried out using the Materials Studio/8 suite's Forcite module, just like our earlier work.⁴⁰ The interactions of all the systems under study were carried out using a simulation box ($27.30 \times 27.30 \times 37.13$ Å³) by the Forcite module in Materials Studio/8. $491\text{H}_2\text{O}$, $9\text{H}_3\text{O}^+$, 9Cl^- , and pyrazole analogues fill this need. With a simulation time of 1000 ps and 1.0 fs and the COMPASS force field, the Andersen thermostat controlled the modeled system's temperature to 303 K in the NVT ensemble.⁴¹

3. RESULTS AND DISCUSSION

3.1. Gravimetric Measurements. **3.1.1. Effect of Concentration.** The influence of L4 and L6 concentrations

Table 2. WL Descriptors for the CS Electrode in 1 M HCl Medium in the Absence and Presence of Diverse L4 and L6 Concentrations at $T = 303 \pm 2$ K

medium	C (M)	C_R (mg/cm ² h)	IE _{WL} (%)	θ
blank	1	2.880 ± 0.060		
	10^{-3}	0.236 ± 0.003	91.8	0.918
L6	10^{-4}	0.276 ± 0.008	90.4	0.904
	10^{-5}	0.469 ± 0.010	83.7	0.837
	10^{-6}	0.662 ± 0.020	77.0	0.770
	10^{-3}	0.285 ± 0.006	90.1	0.901
L4	10^{-4}	0.628 ± 0.020	78.2	0.782
	10^{-5}	0.720 ± 0.030	75.0	0.750
	10^{-6}	0.884 ± 0.020	69.3	0.693

Table 3. Evolution of W and the Corresponding IE_{WL} % with Various Temperatures for CS Immersed in 1 M HCl with and without 10^{-3} M L4 and L6

medium	T (K)	C_R (mg/cm ² h)	IE _{WL} (%)	
blank	303	02.880 ± 0.060		
	313	04.803 ± 0.100		
	323	07.187 ± 0.200		
	333	10.050 ± 0.200		
	303	0.236 ± 0.003	91.8	0.918
L6	313	0.499 ± 0.010	89.6	0.896
	323	1.049 ± 0.030	85.4	0.854
	333	2.231 ± 0.040	77.8	0.778
	303	0.285 ± 0.006	90.1	0.901
L4	313	0.581 ± 0.010	87.9	0.879
	323	1.171 ± 0.030	83.7	0.837
	333	2.402 ± 0.070	76.1	0.761

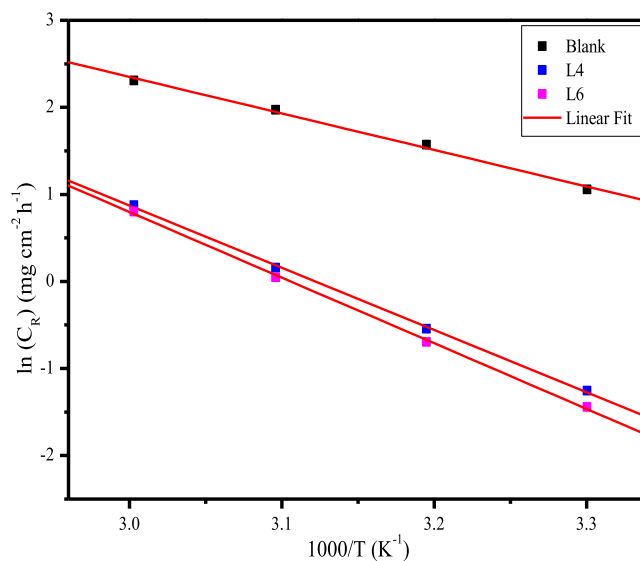


Figure 2. Arrhenius graphs for (CS/1 M HCl) without and with 10^{-3} M L6 and L4.

on the protection performance was evaluated gravimetrically for the CS electrode in 1 M HCl at 303 K. Table 2 displays corrosion rate values (C_R) as well as inhibition activities for each inhibitor concentration (from 10^{-6} to 10^{-3} M). One may

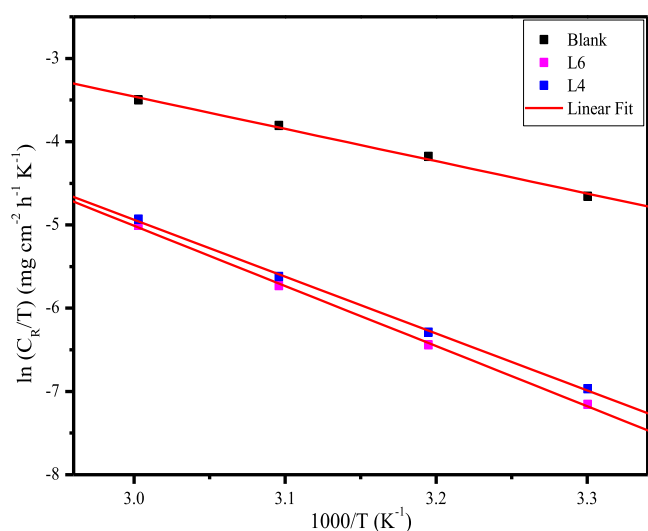


Figure 3. Transition state graphs for (CS/1 M HCl) without and with 10^{-3} M L6 and L4.

Table 4. Thermodynamic Parameters Were Generated for 10^{-3} M L6 and 10^{-3} M L4 in 1 M HCl

C (M)	R^2	E_a (kJ/mol)	ΔH_a^* (kJ/mol)	ΔS_a^* (J/mol K)
blank	0.99775	34.90	32.27	-129.50
10^{-3} M L6	0.99955	62.72	60.09	-58.94
10^{-3} M L4	0.99954	59.48	56.84	-68.05

notice that the corrosion rate subsides with the increase in L4 and L6 concentration. This results in a gradual increase of the inhibition efficiency (IE_{WL} %) reaching maximal values of 90.1 and 91.8% at an optimized concentration of 10^{-3} M L4 and L6, respectively. The difference noticed in the percentage of the IE_{WL} can be attributed to the molecular structure of the L6 inhibitor as it contains additional oxygen atoms. Such heteroatoms have the capacity to form a donor–acceptor surface complexes and thus influence the inhibition efficiency. From these results, it can be suggested that L4 and L6 molecules mitigate the corrosive attack of CS surface subjected to the aggressive electrolyte through their adsorption.

3.1.2. Effect of Temperature. It is acknowledged that temperature significantly alters the conduct of metals in aggressive media as well as the interaction between the metallic substrate and the inhibitory products. In order to assess the impact of temperature on the weight loss trend and its respective inhibition performance, gravimetric trials were conducted for the CS sheet immersed for 6 h with and without 10^{-3} M L4 or L6 compounds in 1 M HCl solution at temperatures in the range of 303–333 K. The WL descriptors are gathered in Table 3. One may be clearly noticed that the increment of temperature induces an increase in C_R values, which negatively affects IE_{WL} %. Earlier studies stated that the coarseness of metallic surfaces increases at higher temperatures, which in turn undermines the inhibitor adsorption on CS.^{42,43} Correspondingly, an increment in temperature affects in a negative way the interaction of both L4 and L6 with the CS surface. Several authors reported that the observed behavior might be the consequence of the low chemical performance of inhibitory molecules as temperature rises, which leads in turn to their desorption from CS surface.⁴⁴

Further details on the adsorption ability of the investigated inhibitors were given through the evaluation of various

activation parameters such as E_a (activation energy), ΔH_a^* (activation enthalpy), and ΔS_a^* (activation entropy). These descriptors were assessed by examining the temperature influence as expressed by the Arrhenius law (eq 8) and transition state formula (eq 9)⁴⁵

$$C_R = A \exp\left(\frac{-E_a}{RT}\right) \quad (8)$$

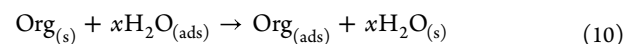
$$C_R = \frac{RT}{Nh} \exp\left(\frac{\Delta S_a^*}{R}\right) \exp\left(\frac{-\Delta H_a^*}{RT}\right) \quad (9)$$

where A denotes the Arrhenius constant, R designates the gas constant, T represents the absolute temperature (K), N denotes Avogadro's number, and h stands for Planck's constant.

The respective graphs are shown in Figures 2 and 3. For both L4 and L6 inhibitors, the Arrhenius plotting depicts straight lines whose slopes are equal to $-E_a/R$. As depicted by Table 4, the derived values of E_a of CS in 1 M HCl containing both L4 and L6 are higher, with respect to the inhibitor-free solution. Hence, it may be postulated that adding L4 or L6 to the medium generates a rise in the energy barrier associated with the corroding process. To put it another way, the corrosion will become less potent on the CS surface and more arduous owing to the obstruction of CS-active centers by L4 or L6 molecules.⁴⁶ Besides, since the activation energy for the L6-containing medium exceeds that for the L4-containing solution, one may assume that the corrosion reaction of CS will possibly be more challenging with the introduction of L6 to the hostile environment.

The positive values of ΔH_a^* emphasize that the generation of the activated complex is accomplished through an endothermic process. Moreover, in the presence of L4 or L6, ΔH_a^* values are greater if compared with the ones estimated in the inhibitor-free solution, demonstrating that the corrosion of CS is mitigated through the addition of the investigated molecules. The negative values of ΔS_a^* indicate the presence of a direct order of the reaction owing to the transformation from reactants to activate complexes.^{45,46}

3.1.3. Adsorption Isotherm. The interaction between organic molecules and metals is generally accomplished by their adsorption on the surface. Such adsorption may be viewed as a quasi-replacement process of H_2O molecules by the organic products in the aqueous phase ($Org_{(aq)}$), as expressed by the subsequent reaction



where x stands for the number of water molecules expelled by the adsorbed inhibitors on the metallic surface.

In general, studies conducted on the adsorption behavior of organic molecules enable us to unravel the mode of action of the inhibitors. The identification of the nature of adsorption usually relies on plotting various adsorption isotherms (Langmuir, Temkin, and Frumkin) in order to ascertain the most appropriate one. As depicted in Figure 4, the Langmuir isotherm exhibits an almost unitary correlation for both L4 and L6 inhibitors. The formula expressing the Langmuir isotherm is denoted by eq 11⁴⁷

$$\frac{C}{\theta} = \frac{1}{K_{ads}} + C \quad (11)$$

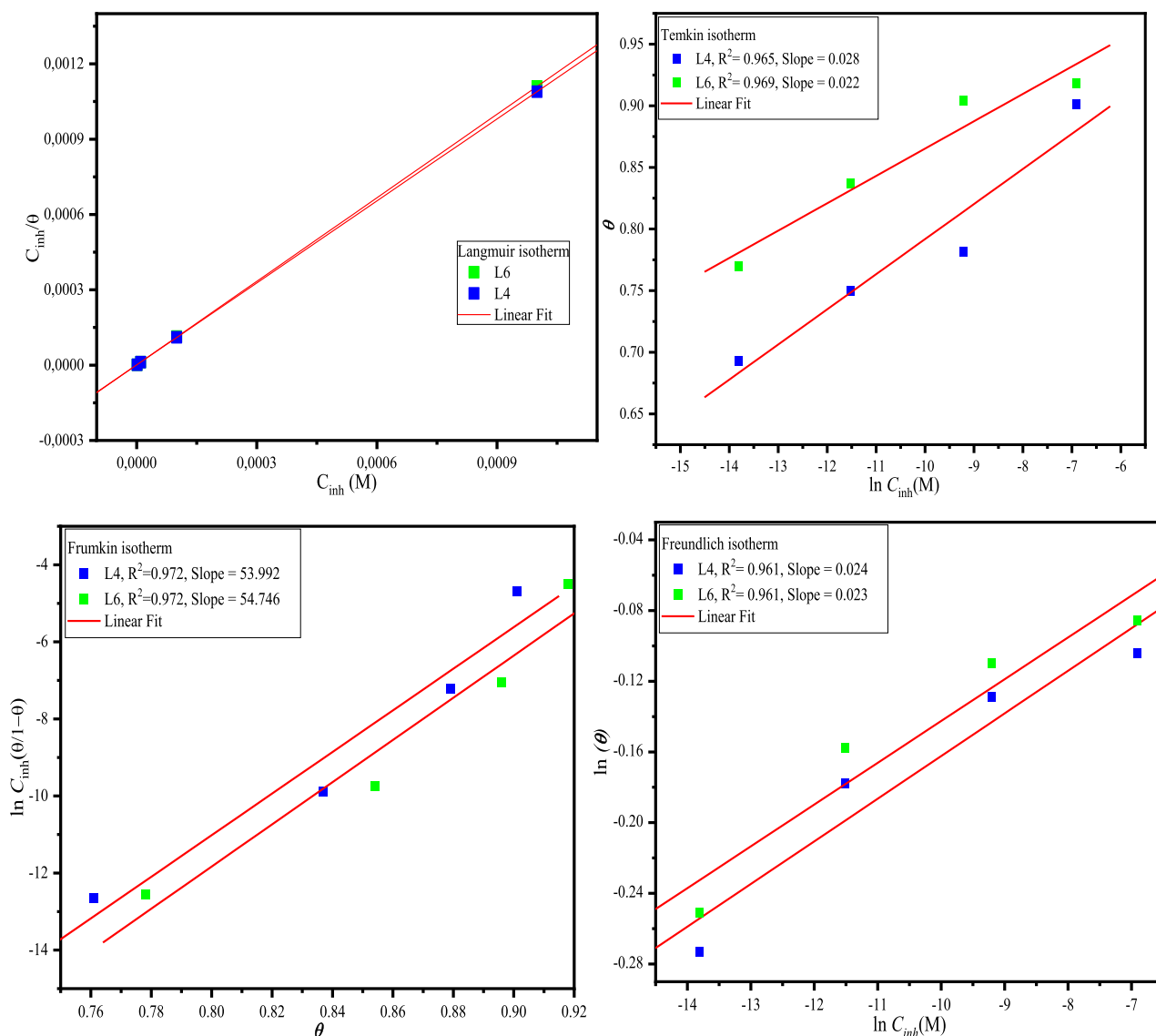


Figure 4. Isotherm models for adsorption of L4 and L6 on the CS surface in 1 M HCl.

Table 5. Thermodynamic Descriptors Resulting from the Langmuir Isotherm Plot for the {L4 and L6/CS/1 M HCl} System

medium	slope	R ²	K _{ads} (L/mol)	ΔG _{ads} * (kJ/mol)
L4	1.10	0.9999	156150.21	-40.24
L6	1.08	0.9999	1009018.6	-44.94

where K_{ads} denotes the adsorption/desorption equilibrium constant and C stands for L4 or L6 concentration in the medium. The high values of K_{ads} emphasize the potent adsorption of both of the tested inhibitors. Accordingly, on the basis of weight-loss measurements, one may deduce that L4 and L6 are monolayers adsorbed on CS.

To gain further understanding of the L4 and L6 adsorption mechanisms on CS, the values of the standard adsorption free energy (ΔG_{ads}) were assessed through eq 12⁴⁸

$$\Delta G_{\text{ads}} = -RT \ln(55.5 K) \quad (12)$$

where R designates the gas constant and T stands for the absolute temperature (K). The 55.5 value denotes the H₂O concentration in the solution (mol/L).

As disclosed in Table 5, the negative values of ΔG_{ads} point out that the layers adsorbed on the CS surface are stable.⁴⁸ For both L4 and L6, the derived values of ΔG_{ads} are close to -40 kJ/mol [ΔG_{ads} (L4) = -40.24 kJ/mol and ΔG_{ads} (L6) = -44.94 kJ/mol]. Therefore, the adsorption of both molecules occurs through electron transfer between L4 or L6 and the CS surface to create a covalent bond (chemical adsorption).⁴⁹

3.2. Electrochemical Measurements. 3.2.1. PDP Curves.

Corrosion kinetics of CS in 1 M HCl solution with and without varying concentrations of L4 and L6 were evaluated through PDP plots drawn under stationary conditions after 30 min of immersion at corrosion potential (E_{corr}) and $T = 303$ (± 2) K. The acquired data are depicted in Figure 5, while the corresponding electrochemical kinetic descriptors, explicitly E_{corr} , corrosion current density (i_{corr}), the anodic Tafel slope (β_a), and the cathodic Tafel slope (β_c), derived from the extrapolation method, are illustrated in Table 6. From Figure 5, one may observe that the progressive introduction of both L4 and L6 to the medium gives rise to a prominent subsidence of the anodic and cathodic partial current densities. This reflects the attenuation of the CS anodic dissolution and the cathodic generation of H₂. The cathodic branches exhibit parallel lines

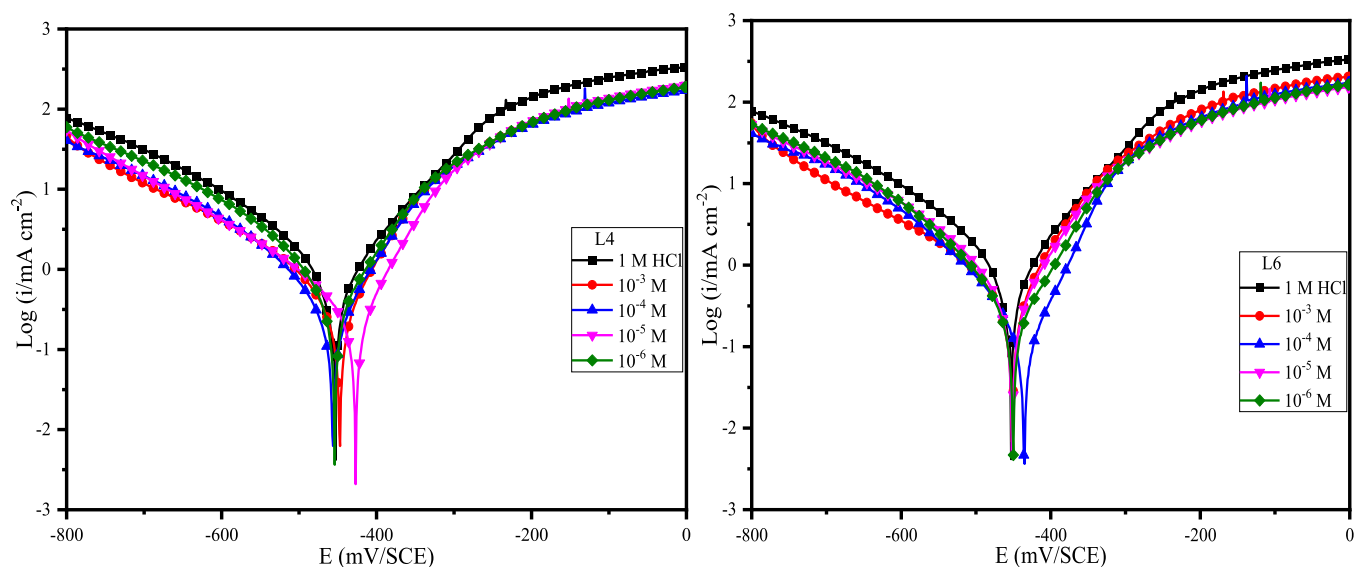


Figure 5. PDP plots for CS in 1 M HCl in the absence and presence of diverse concentrations of L4 and L6.

Table 6. PDP Descriptors for CS in 1 M HCl (Blank) and with Various L4 and L6 Concentrations at $T = 303 \text{ K} (\pm 2)$

system	C (M)	$-E_{\text{corr}}$ (mV/SCE)	i_{corr} ($\mu\text{A cm}^{-2}$)	β_a (mV dec $^{-1}$)	$-\beta_c$ (mV dec $^{-1}$)	R_p ($\Omega \text{ cm}^2$)	IE _{POL} (%)
blank	1	456.3 \pm 6	1104.1 \pm 4.9	112.8	155.4	25.7	
L4	10 $^{-3}$	448.5 \pm 3	158.5 \pm 1.6	73.3	83.1	106.7	85.6
	10 $^{-4}$	453.7 \pm 2	290.8 \pm 2.1	77.3	114.8	69.0	73.6
	10 $^{-5}$	426.5 \pm 4	324.7 \pm 2.5	70.4	150.3	64.1	70.6
	10 $^{-6}$	452.4 \pm 4	396.3 \pm 3.0	79.8	98.9	48.4	64.1
	10 $^{-3}$	449.9 \pm 3	143.2 \pm 1.3	63.2	82.5	108.5	87.0
L6	10 $^{-4}$	428.3 \pm 5	155.6 \pm 1.4	70	106.7	118.0	85.9
	10 $^{-5}$	444.9 \pm 5	234.6 \pm 2.0	68.2	87.9	71.1	78.7
	10 $^{-6}$	448.7 \pm 2	302.5 \pm 2.9	85.4	114	70.1	72.6

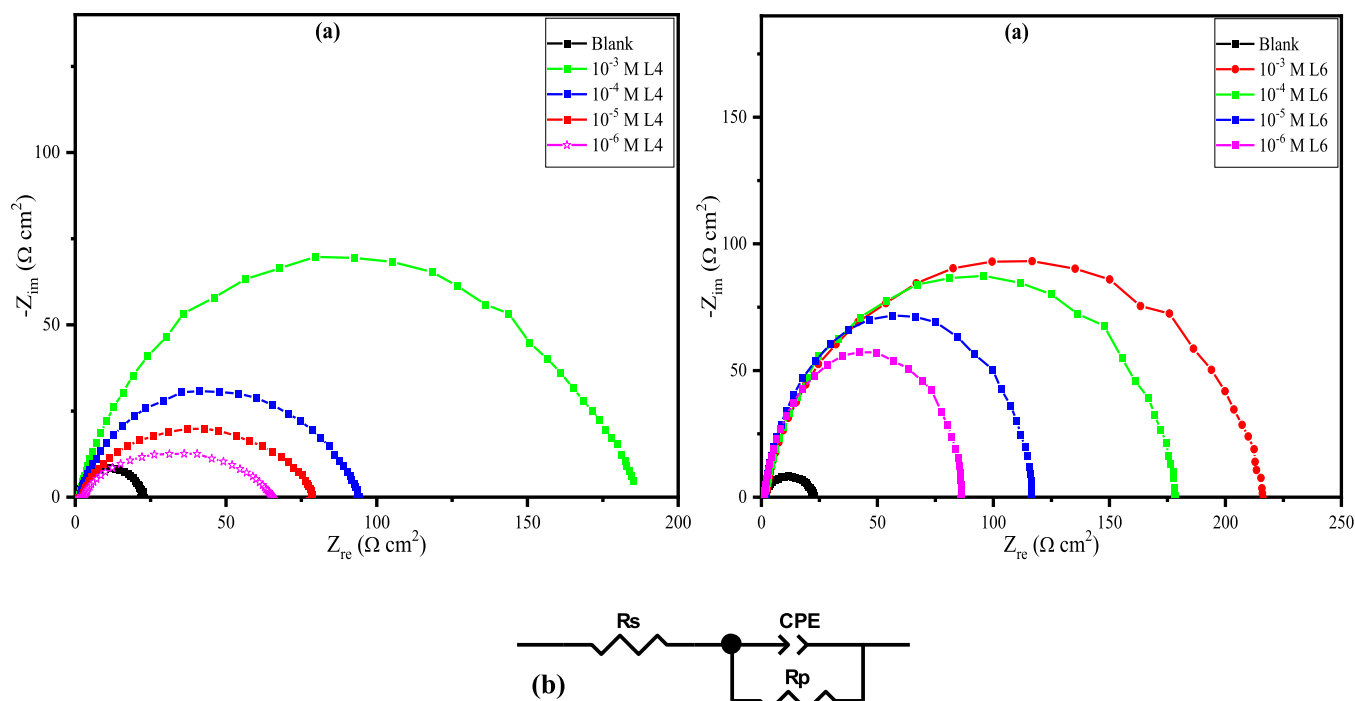


Figure 6. (a) Nyquist diagrams of CS in inhibitor-free 1 M HCl solution and with the addition of various concentrations of L4 and L6 at $303 \pm 2 \text{ K}$ and (b) the corresponding electrical circuit employed for fitting the EIS spectra.

Table 7. Electrochemical Impedance Descriptors of CS in 1 M HCl Solution Comprising Varied Concentrations of L4 and L6 at 303 ± 2 K

system	C (M)	R_s (Ω cm ²)	R_p (Ω cm ²)	$10^6 \times Q$ (μ F sn ⁻¹ cm ⁻²)	n	C_{dl} (μ F cm ⁻²)	IE _{EIS} (%)
blank	1	0.83 ± 0.06	21.6 ± 0.6	293.9 ± 5.8	0.845 ± 0.001	116.2	
L6	10 ⁻³	1.32 ± 0.03	215.9 ± 4.3	072.2 ± 6	0.865 ± 0.002	033.7	89.9
	10 ⁻⁴	1.25 ± 0.04	177.3 ± 5.3	131.6 ± 6	0.858 ± 0.001	070.6	87.7
	10 ⁻⁵	1.12 ± 0.01	116.8 ± 2.3	188.7 ± 6	0.843 ± 0.005	092.7	81.4
	10 ⁻⁶	0.95 ± 0.02	086.0 ± 0.9	220.0 ± 6	0.834 ± 0.003	099.9	74.7
L4	10 ⁻³	1.14 ± 0.03	185.5 ± 3.7	075.2 ± 6	0.890 ± 0.002	044.3	88.2
	10 ⁻⁴	1.09 ± 0.02	093.7 ± 1.0	134.6 ± 6	0.873 ± 0.002	071.2	76.8
	10 ⁻⁵	0.98 ± 0.01	078.7 ± 0.8	191.7 ± 6	0.858 ± 0.005	095.7	72.4
	10 ⁻⁶	0.91 ± 0.01	065.2 ± 0.7	223.1 ± 6	0.843 ± 0.006	101.5	66.7

for both L4 and L6 molecules, emphasizing that the L4 and L6 presence in the solution does not adjust the process of hydrogen production. It can be then suggested that the reduction of hydrogen ions on CS is predominantly achieved via the electron-transfer mechanism (pure activation process).⁵⁰ In the presence of each inhibitor (L4 and L6), the anodic Tafel segments above -300 mV exhibit approximately identical conductivities for each of the studied concentrations. However, the anodic current densities are still lower for each inhibitory concentration compared to the one drawn in a blank 1 M HCl solution. This is primarily driven by the significant dissolution of the CS-inducing desorption of the inhibitors. In this case, it might be suggested that the rate of desorption of L4 and L6 molecules is higher compared to their adsorption.

A review of Table 6 reveals a progressive subsidence of i_{corr} values as L4 and L6 concentrations increase in the medium. Furthermore, a subtle displacement of E_{corr} is depicted toward more positive values with the introduction of L4 and L6 in the solution. Riggs reported that organic products may be classified as anodic or cathodic inhibitors in case E_{corr} shifts at least 85 mV regarding the potential found molar HCl.⁵¹ As indicated in Table 6, the differences of E_{corr} values ($\Delta E_{corr} = 7.8$ mV for the system {CS/1 M HCl/10⁻³ M L4} and 6.4 mV for {CS/1 M HCl/10⁻³ M L6}) are lower than 85 mV, confirming the mixed character of both L4 and L6.^{52,53} In addition, the reported variation in Tafel slopes (β_a and β_c) values upon the presence of L4 or L6 denotes that the tested inhibitors tend to minimize the corrosion-sensitive specific surface area and alter the corrosion pathway, presumably through the blockage of the reaction centers on CS surface by L4 and L6 molecules.⁵⁴

Furthermore, the value of the Stern–Geary coefficient B [$B = \beta_a \times \beta_c / 2.303 (\beta_a + \beta_c)$] does not change remarkably. Note that this coefficient associates with the corrosion rate and the polarization resistance ($R_p = B/i_{corr}$). Accordingly, it can be noticed that R_p values determined by the calculation of the Stern–Geary coefficient are very close to those assessed by EIS measurements (Section 3.2.2), thus reflecting the consistency of the results obtained by both electrochemical methods.

The inhibition activities IE_{POL} (%), assessed from PDP plots by eq 1, increase significantly with increasing L4 and L6 concentration, reaching maximal values of IE_{POL} (L4) = 85.6% and IE_{POL} (L6) = 87% for a concentration of 10⁻³ M. The slight increase of IE % achieved for L6 compared to that for L4 can be associated with the increment of electron transfer owing to the functionalization by the carboxylate group in the L6 compound. Further insights will be given by theoretical studies. The aforementioned outcomes further substantiate that the adsorption of L4 or L6 on the Fe-CS/1 M HCl complex can proficiently obstruct the active centers on CS and subsequently

preclude corrosion. The PDP findings are consistent with the favorable outcomes derived from gravimetric trials.

3.2.2. EIS Data. The Nyquist spectra for CS at E_{corr} in 1 M HCl at 303 K with and without L4 and L6 inhibitors are evinced in Figure 6a, whereas the related EIS descriptors are gathered in Table 7. For all concentrations, Nyquist curves show the presence of a unique flattened semicircle, which reveals that CS corrosion is a process controlled by a single charge transfer⁵⁵ in the absence or presence of the inhibitors in the aggressive solution. A wider radius of the loops with the increment of L4 or L6 inhibitory concentration points out an increase of the electron-transfer mechanism,^{56,57} which reflects in turn the development of a dense anticorrosion film (mono- or multilayer) on the CS electrode surface, restraining hence the deterioration of the electrode effectively.⁵⁸

Figure 6b depicts the equivalent circuit used to adjust EIS data recorded for the {1 M HCl/L4 or L6/CS} system, where R_s refers to the aqueous solution resistance, R_p designates the resistance of polarization, paralleling a constant phase element (CPE) referring to the capacitance of the electrical double layer (C_{dl}) at the interface CS/1 M HCl. The impedance function of a CPE (taking into account a nonideal capacitive response on a heterogeneous surface) is described by eq 13

$$Z_{CPE} = Q^{-1}(i\omega)^{-n} \quad (13)$$

where Q , i , ω , and n denote, respectively, the CPE constant, imaginary number ($i^2 = -1$), angular frequency ($\omega = 2\pi f$), and phase shift. n designates the divergence with respect to the ideal conduct, comprised between 0 and 1. As claimed by MacDonald,⁵⁹ the value of n gives an indication of the substrate heterogeneity. For instance, n is homologous to a resistance when $n = 0$, a capacitor for $n = 1$, and assigned to a diffusion process when $n = 0.5$.

From CPE parameters, the double capacitance values C_{dl} were assessed according to eq 14

$$C_{dl} = (Q \times R_p^{1-n})^{1/n} \quad (14)$$

Table 7 discloses the derived EIS indices: R_p , n , C_{dl} , and the inhibition efficiencies IE_{EIS} (%). The subtle increase of n values with the progressive addition of both L6 and L4 molecules, if compared to the inhibitor-free electrolyte, could be attributable to a lower level of surface coarseness of the electrode.⁶⁰ This can be a consequence of the development of a barrier layer on the CS substrate. A review of Table 7 unveils that C_{dl} values consistently subside with the gradual addition of L4 or L6 molecules, which might be attributed to a lowering of local dielectric constant along with CS exposure and/or an apparent increment in the electrical double-layer thickness.⁶¹ One might be suggested that the observed trend might be allocated to the

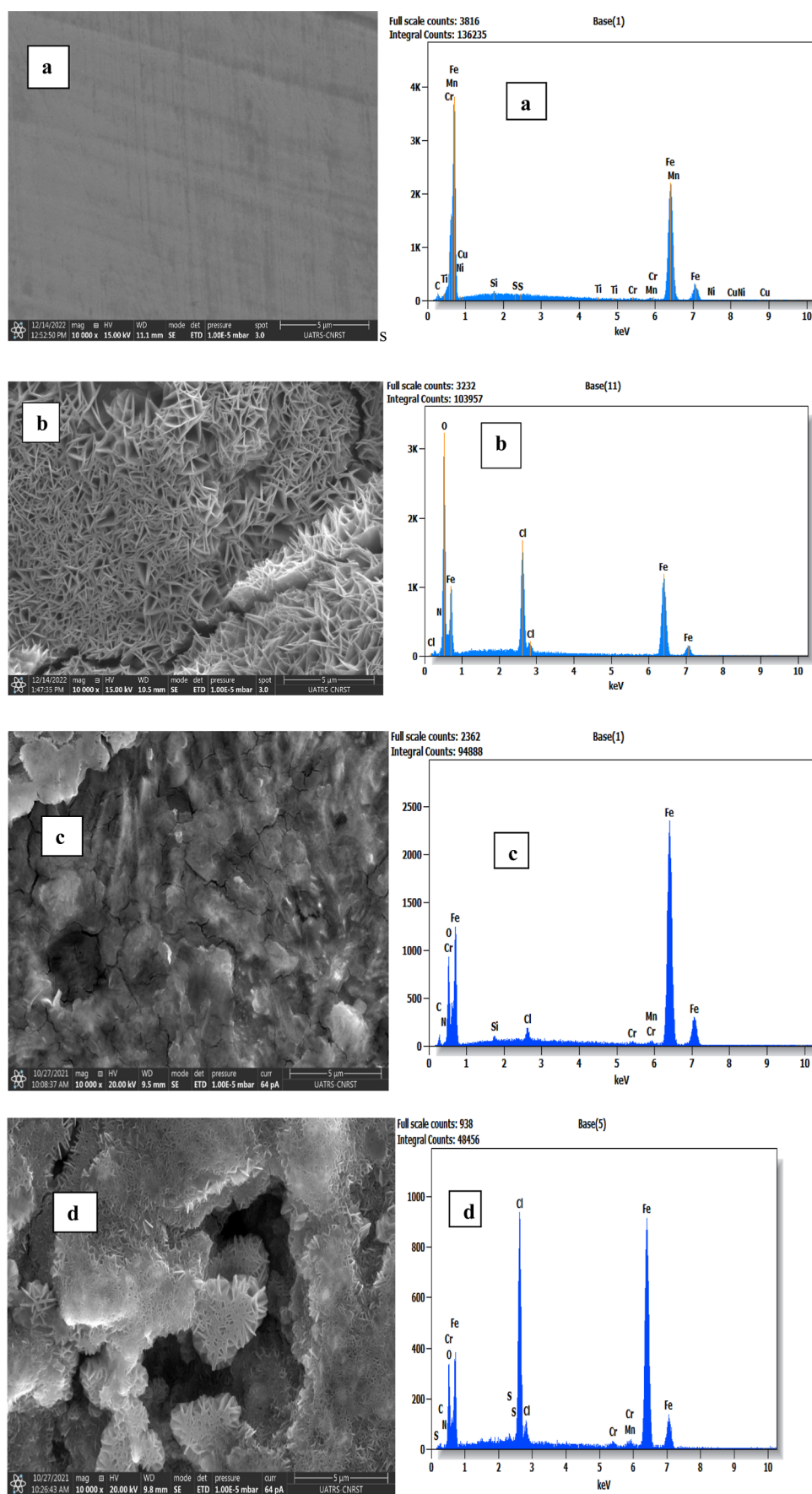


Figure 7. SEM micrographs and their related EDX analysis of CS specimens (a) before immersion, (b) after 24 h immersion in 1 M HCl, (c) 1 M HCl + 10^{-3} M L4, and (d) 1 M HCl + 10^{-3} M L6 at 303 K.

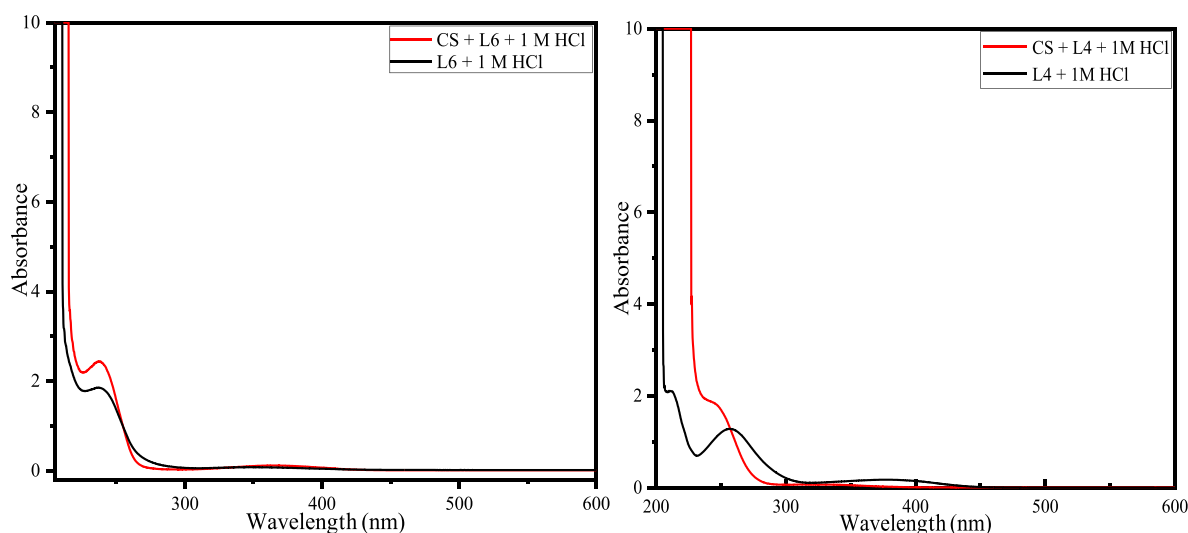


Figure 8. UV–visible spectra of 10^{-3} M L4 and L6 compounds added to 1 M HCl with and without CS.

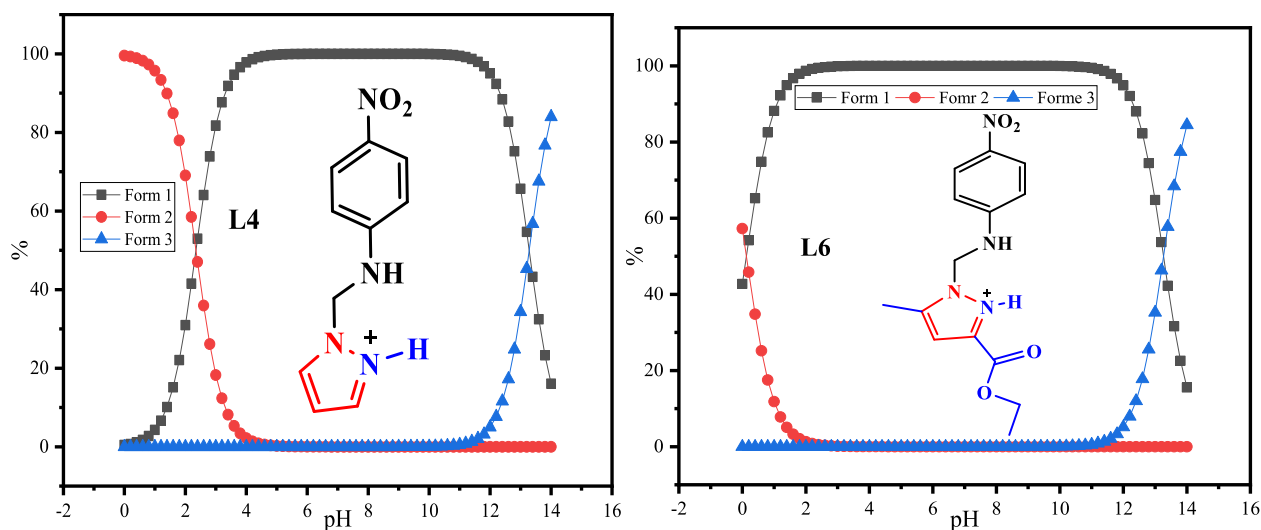


Figure 9. Protonation site defined by its percentage vs pH of L4 and L6.

coverage of the metal surface by L4 or L6 molecules. This coverage may be induced by the adsorption of the organic pyrazole molecules on CS through the displacement of H_2O from the surface, thus ensuring a significant decrease in CS dissolution.⁶²

In this work, R_p values were estimated instead of those of R_{ct} . R_p gives more accurate insights into the inhibition process as it takes into account both charge-transfer resistance R_{ct} and film resistance R_f ($R_p = R_f + R_{ct}$). According to Table 7, R_p values exhibit a remarkable increment as the L4 or L6 concentration increases. Thus, one can assume that the progressive introduction of L4 or L6 into 1 M HCl solution enhances R_{ct} values. Indeed, higher R_{ct} values reflect the delay of the charge-transfer process due to the development of protective films of L4 or L6 by adsorption on the CS substrate.

Based on the above findings, the inhibition activity IE_{EIS} (%) values show an enhancement with increasing inhibitory concentration $\{\text{IE}_{\text{EIS}}$ (L4) = 89.9% and IE_{EIS} (L6) = 88.2% for a concentration of 10^{-3} M}. A small increase in IE_{EIS} % evaluated for L6 is noticed when compared to the one assessed for the L4 inhibitor. Note that a similar trend was discerned through PDP measurements and weight-loss data. Therefore, it

is possible to conclude that both tested inhibitors impart efficient protection against CS corrosion in the HCl environment.

3.3. SEM/EDX Analysis. CS specimens were inspected by SEM before immersion (Figure 7a) and maintained immersed for 24 h at 303 K in 1 M HCl without (Figure 7b) and with the introduction of 10^{-3} M L4 (Figure 7c) and 10^{-3} M L6 (Figure 7d). Except for the appearance of some polishing scratches, no discernible defects are visible on the SEM image of sanded CS. After immersion in 1 M HCl for 24 h, the CS surface undergoes severe corrosion, as witnessed by the formation of a rust layer with a flowery structure with fine plates. The related EDX spectrum evinces the occurrence of high peaks of Cl and O atoms, which may possibly correspond to the presence of FeCl_2 and Fe_3O_4 as corrosion products.⁶³ This emphasizes that the CS substrate undergoes general corrosion in 1 M HCl. Following the addition of 10^{-3} M L4 and L6 inhibitors, the surface is capped with a platelet-shaped compound, indicating the development of an adsorbed protective layer. In the presence of inhibitors, the EDX spectra depict peaks of the O atom (adsorption of L4 and L6), while the Cl peak contribution (mostly coming from the solution) is significantly

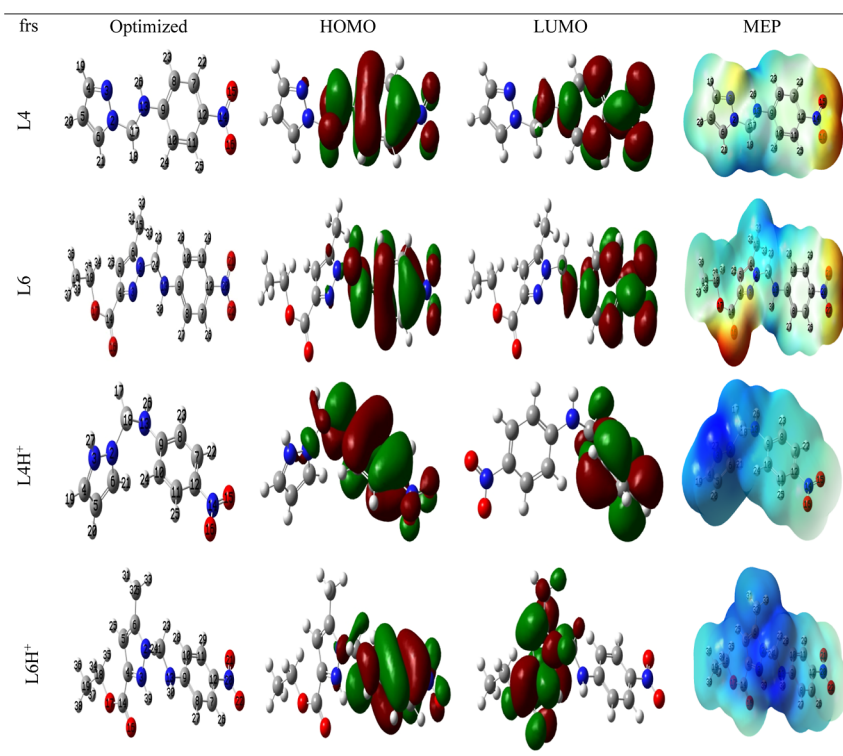


Figure 10. Energy-minimized structures, FMOs, and MEPs of the two neutral and protonated forms for L4 and L6 and L4H⁺ and L6H⁺.

Table 8. Descriptors for Reactivity of the L4, L6, L4H⁺, and L6H⁺

molecules	E_{HOMO} (eV)	E_{LUMO} (eV)	ΔE (eV)	X (eV)	H (eV)	ΔN_{110}
L4	-6.223	-2.016	4.207	4.119	2.103	0.167
L6	-6.372	-2.095	4.277	4.233	2.138	0.137
L4H ⁺	-9.763	-5.703	4.060	7.733	2.030	-0.717
L6H ⁺	-9.779	-5.953	3.826	7.866	1.913	-0.796

diminished. On the basis of these observations, it can be suggested that both L4 and L6 have great protective abilities as they impede the electrolyte accessibility to CS specimens through the formation of a stable and adherent deposit.

3.4. UV–Visible Investigation. Further insights into the interaction of CS and the inhibitory molecules were gained through UV–visible spectroscopic measurements. The latter was conducted in 1 M HCl solution enclosing 10^{-3} M of either L4 or L6 before and after immersion in the CS for 72 h at 303 K (Figure 8). The absorption curves of the studied inhibitory compounds before CS immersion (black curve) depict two visible bands around 211 and 258 nm for L4 and a single band at 240 nm for L6. After 72 h of CS immersion, one may notice a shift to a higher value (247 nm) and the disappearance of the second band (located at 258 nm before CS immersion) in the case of L4 inhibitor, whereas a very slight displacement of the band to 238 nm and an increase in its maximum (λ_{max}) are shown for L6 inhibitor. This emphasizes the interaction (production of a complex) between the investigated pyrazole compounds and Fe²⁺ ions in the aggressive solution.^{64,65}

3.5. DFT Reactivity. To explore the corrosion inhibition efficiency and offer a potential corrosion inhibition mechanism, a set of the electronic characteristics, global reactivity descriptors, and local reactivity indices of the neutral (L4

and L6) and protonated (L4H⁺ and L6H⁺) forms were determined.⁶⁶

To better understand the reactivity of L4 and L6 in the protonated state, we have presented the results of Marvin sketch software.^{67,68}

Figure 9 presents the variation of protonation % vs pH of L4 and L6. As analyzed in this figure, the nitrogen atom hybridized sp² and included in the pyrazole ring protons with a high percentage for two molecules, which makes the molecules positively charged as cations.

The absence of imaginary frequencies with the use of the same degree of theory is required to ensure the compliance of the structure. The molecular forms' structures, highest occupied molecular orbitals (HOMOs), and lowest unoccupied molecular orbitals (LUMOs), were traced using the GaussView/5 program.

Figure 10 depicts the energy-minimized structures, frontier molecular orbitals (FMOs), and molecular electrostatic potentials (MEPs) of two neutral and protonated forms, L4 and L6 and L4H⁺ and L6H⁺. The electronic representations of HOMO and LUMO show that the neutral forms L4 and L6 are occupied in the structural part of methyl-4-nitroaniline. In contrast, the FMOs for L4H⁺ and L6H⁺ have an almost total occupation except for a few atoms, implying that the reactivity is very high with other species and especially with the metal surface.

E_{HOMO} and E_{LUMO} values serve to analyze the donor/acceptor ratio in the molecule/metal relationship.⁶⁹ In this investigation of quantum computation, the behavior of the reactivity of the two considered neutral (L4 and L6) and charged (L4H⁺ and L6H⁺) forms is followed by the two descriptors. Table 8 shows the different values of the reactivity descriptors of these molecules.

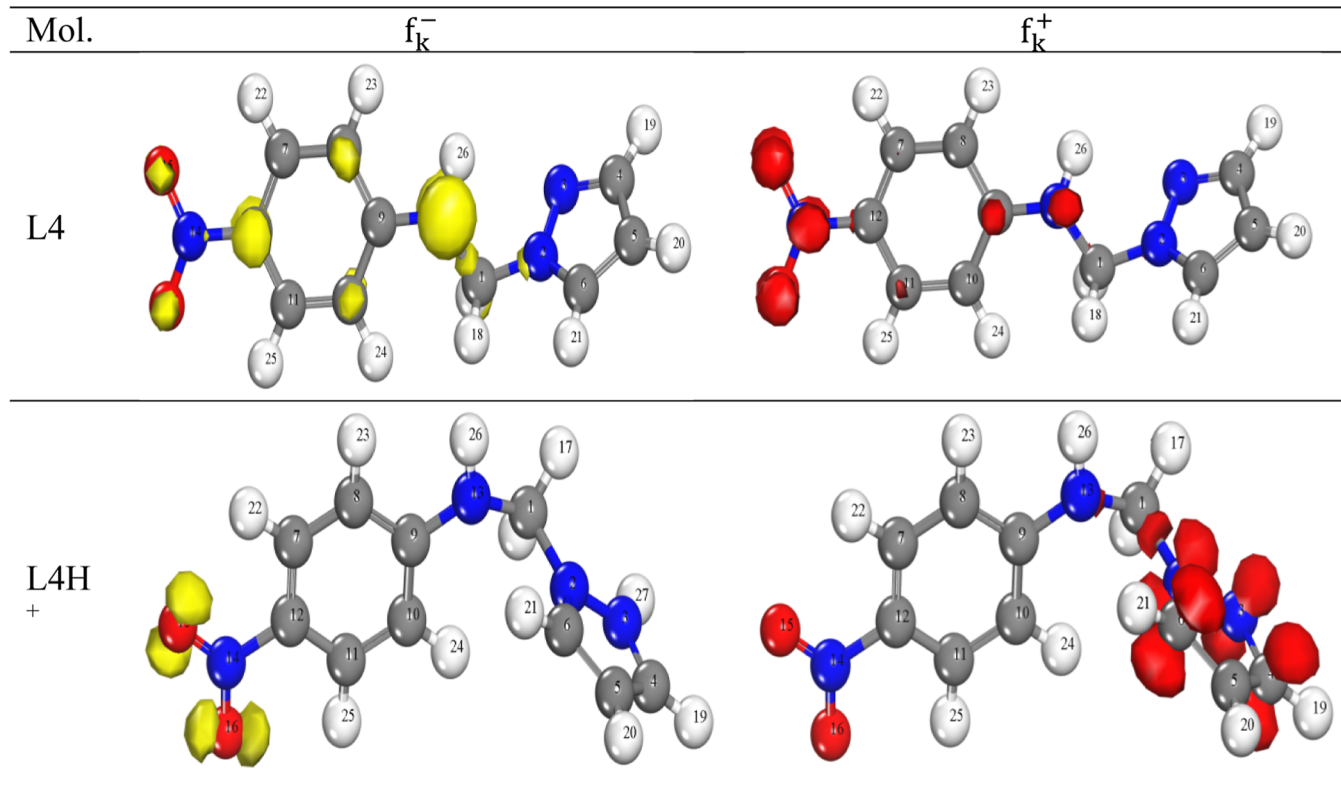


Figure 11. 3D Isosurfaces of the Fukui functions (isosurface density) for the neutral (L4) and protonated (L4H⁺) inhibitors.

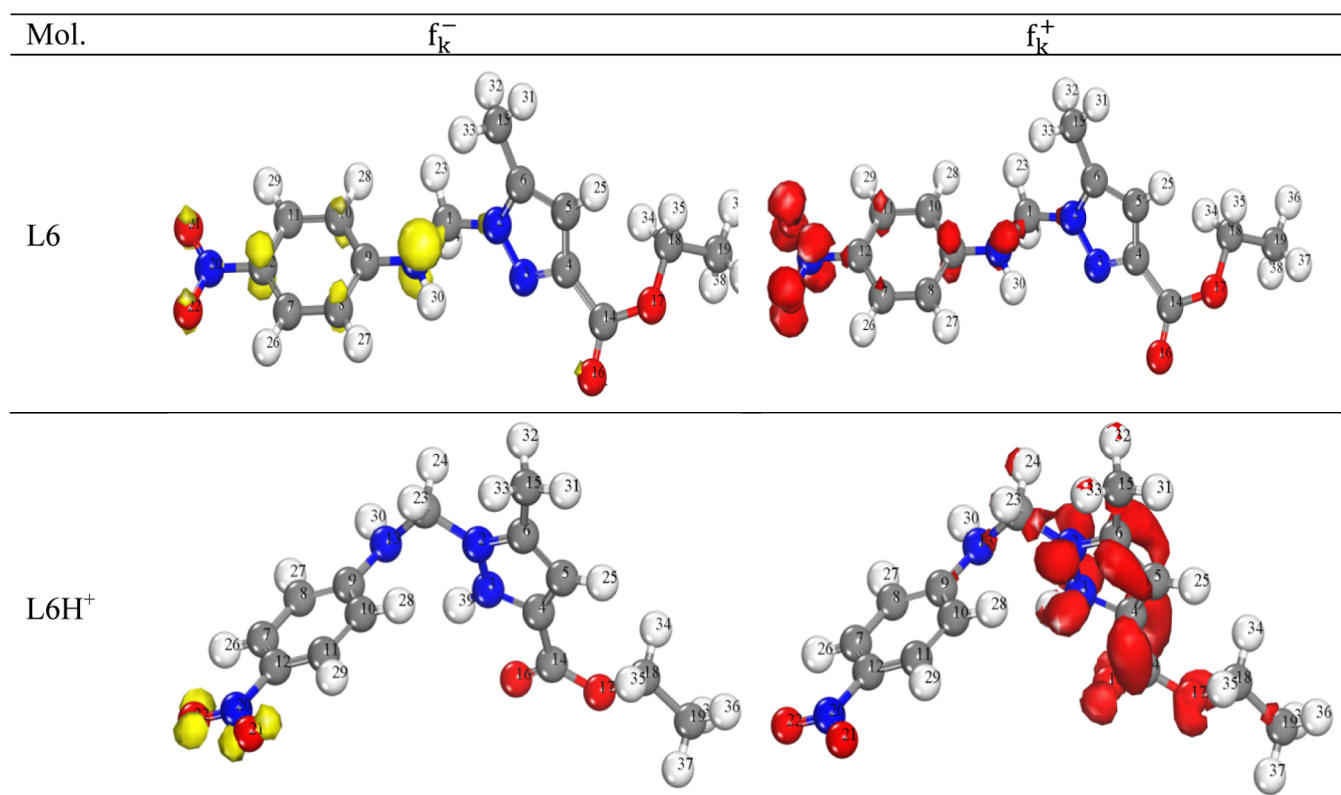


Figure 12. 3D Isosurfaces of the Fukui functions (isosurface density) for the neutral (L6) and protonated (L6H⁺) inhibitors.

The data in Table 8 reveal that the L4 molecule is more nucleophilic ($E_{\text{HOMO}} = -6.223$ eV) and the L6H⁺ molecule is more electrophilic ($E_{\text{LUMO}} = -5.953$ eV).

As the least significant value of this descriptor, ΔE ($E_{\text{LUMO}} - E_{\text{HOMO}}$) enables us to quantify the reactivity of a molecule, and this particular reactivity is the greatest.

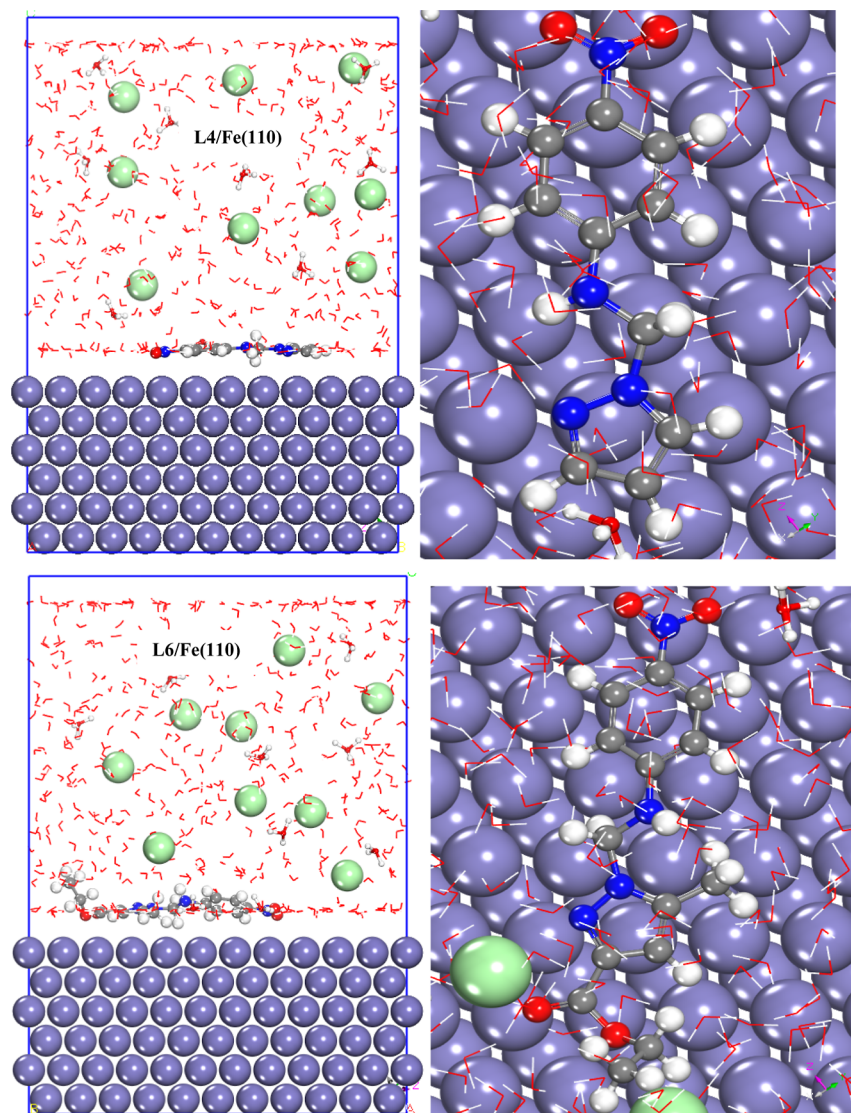


Figure 13. Side (left) and top (right) views of the L4/Fe(110) and L6/Fe(110) systems.

The description comparison between all values of this descriptor shows that the charged form $L6H^+$ is more reactive, with a low value of 3.826 eV. Therefore, $\Delta E(L6) > \Delta E(L4)$ implies that L4 is more reactive than L6, which does not support the experimental findings. However, the order of ΔE for the protonated forms confirms the experimental results.

The electronegativity (X) presents an attractive power of the electrons of a chemical species; the high value of X indicates a high interaction between the inhibitor and iron surface.⁷⁰ The value of 7.866 eV of L6 posted in Table 8 shows this more reactive form.

The fraction of electrons transferred (ΔN_{110}) values provides useful information on the tendency of the electrons to flow from the inhibitor molecule to the CS surface ($\Delta N > 0$) or from the CS to the inhibitor ($\Delta N < 0$).⁷¹

In this computation, the L4 molecule ($\Delta N_{110} = 0.176$) is more likely to share its electron to form coordination bonds with Fe(110). In contrast, $L4H^+$ and $L6H^+$ do not show this attitude, which may be influenced by protonation of the nitrogen atom.

The chemical quantum descriptors of the neutral forms do not show a correlation with the experimental results, whereas

these descriptors for the protonated forms are in good agreement with the inhibitory efficacy values of L4 and L6 $\Delta E(L4H^+) > \Delta E(L6H^+)$, $X(L6H^+) > X(L4H^+)$, $\eta(L4H^+) > \eta(L6H^+)$, etc. The reactivity of $L6H^+$ is higher than that of $L4H^+$, possibly due to the ester group of the protonated L6 form. This shows that the protonated form is more likely to be dominant in the acidic environment.

The Fukui function analysis was utilized to estimate the nucleophilic (f_k^+) and electrophilic (f_k^-) assaults caused by the two forms' most active centers in order to better understand how the L4, L6, $L4H^+$, and $L6H^+$ adsorb onto the CS (Figures 11 and 12).⁷²

This approach was carried out using the Dmol³ method with the GGA correlation exchange functional and the DNP base, as reported in the work published by Benhiba et al.⁷² The calculation data for all forms are listed in Tables S1 and S2, as well as 3D isosurfaces of the Fukui functions (isosurface density) for the neutral (L4 and L6) and protonated ($L4H^+$ and $L6H^+$) inhibitors. It has been ascertained that the neutral form of L4 contains several electron donor and attractor sites that efficiently enhance the reactivity of this molecule. This shows that L4 is more effective against the corrosion of the

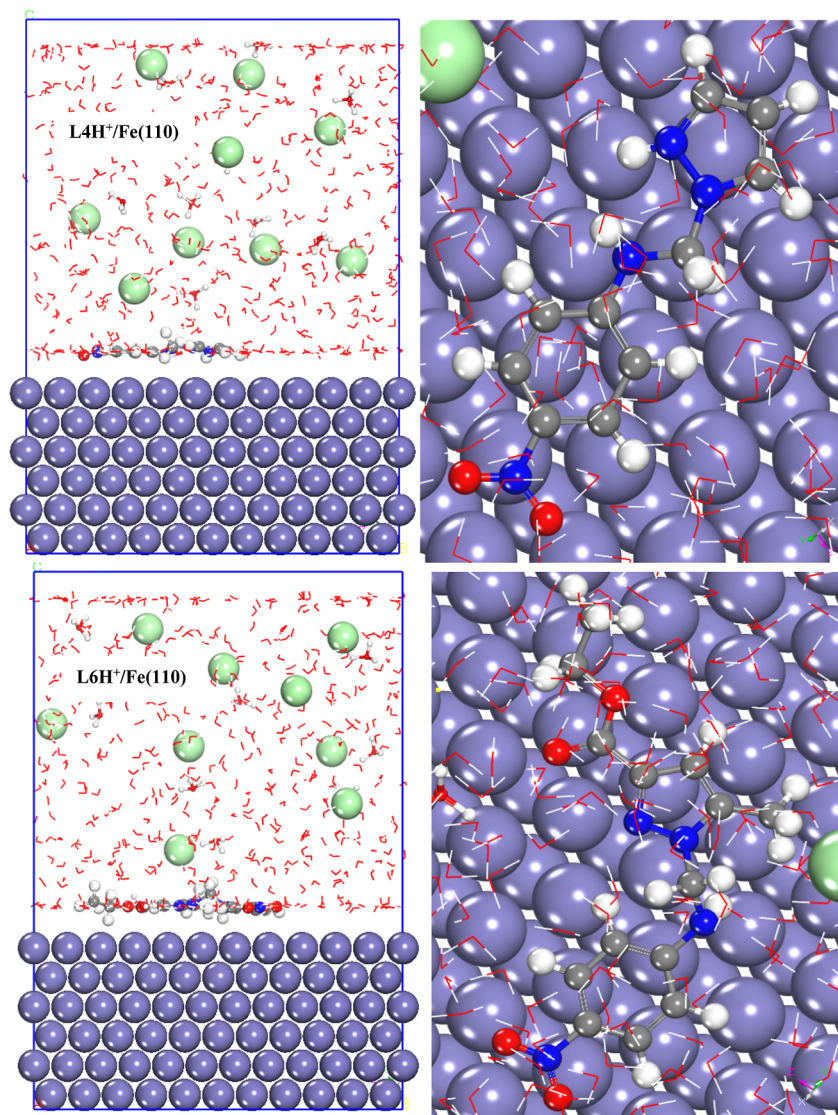


Figure 14. Side (left) and top (right) views of the L4H⁺/Fe(110) and L6H⁺/Fe(110) systems.

Table 9. E_{inter} for the Systems L4/Fe(110), L6/Fe(110), L4H⁺/Fe(110), and L6H⁺/Fe(110) (in kJ mol⁻¹)

systems	$E_{\text{interaction}}$
L4/Fe(110)	-778.604
L6/Fe(110)	-755.431
L4H ⁺ /Fe(110)	-772.529
L6H ⁺ /Fe(110)	-774.648

studied steel and results in a greater number of available coordination bonds enhancing the adsorption of the L4 onto the Fe support. For charged forms, the local reactivity arises and increases by the attractor effect due to the protonation, i.e., the attractor sites are very substantial.

3.6. MD Simulation Study. The adsorption pattern of a molecule onto a metal can be predicted and understood with the aid of computational approaches such as MD simulations. The MD is an effective instrument for examining the behavior of molecular systems as well.⁷³ The current research aims to assess and comprehend the behavior of the L4, L6, L4H⁺, and L6H⁺ molecules on the iron atomic support (Fe(110)). Furthermore, Figures 13 and 14 reproduce the best adsorption configuration of the two forms onto the Fe(110) surface. The

optimal arrangement of the L4, L4H⁺, and L6H⁺ molecules occupies a sizable portion of the Fe(110), as shown in these two pictures. This demonstrates that the simulated molecule contains more reactive sites that are concentrated in the region of the molecule that is filled with FMO (HOMO _ LUMO) iron atoms and has a high potential to adsorb onto the metal due to the presence of coordination bond inhibitors, such as Fe(110). However, the L6 molecule carries a few motifs and atoms that do not interact with the first layer of Fe(110). This suggests that this inhibitor is less reactive than the other species.

The $E_{\text{interaction}}$ (E_{inter}) value is defined by the equation hereunder⁷⁴

$$E_{\text{inter}} = -E_{(\text{surface}+\text{solution})} - E_i + E_{\text{total}} \quad (15)$$

The low value of E_{inter} confirms interactions between all forms and the iron atoms.⁷⁵ Table 9 lists the values of this descriptor for all systems. Based on a comparison analysis, it seems that the largest negative value of L4/Fe(110) (-778.604 kJ mol⁻¹) indicates a more significant interaction. As a result, the data from this simulation support the findings of the experimental investigation and DFT.

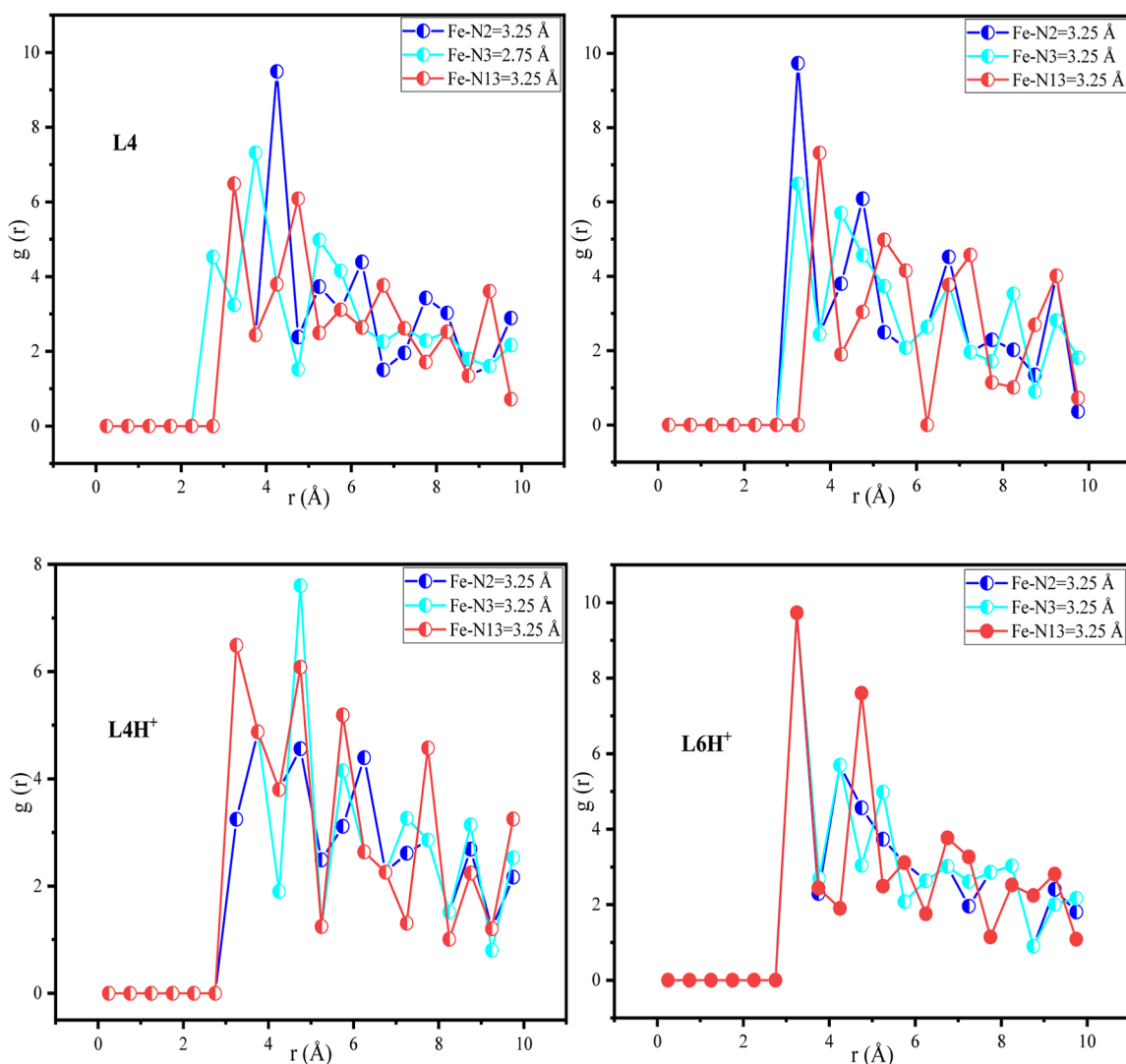


Figure 15. RDFs for L4-Fe, L6-Fe, L4H⁺-Fe, and L6H⁺-Fe.

Consequently, as shown in the DFT section, the protonated form of L6H⁺ exhibits high reactivity (interaction) with the Fe(110) surface, confirming the experimental results.

This method's primary objective was to enter the radial distribution function ("RDF") in order to evaluate the acceptability of the interatomic distances for L4-Fe, L6-Fe, L4H⁺-Fe, and L6H⁺-Fe for adsorption.⁷⁶ The published literature confirmed that the likelihood of chemical adsorption was higher when the bond length was less than 3.5 Å. By contrast, physical adsorption is more probable.⁷⁶ In Figure 15, the spectral data from this method is illustrated. The first peaks reveal that the bond lengths for L4-Fe, L6-Fe, L4H⁺-Fe, and L6H⁺-Fe are less than 3.5 Å.

4. CONCLUSIONS

Two pyrazole derivatives, L4 and L6, were employed to alleviate the corrosion of CS in HCl medium. According to the electrochemical tests, the inhibitors act in a mixed-type process of CS corrosion. L6 exhibits a much better inhibitive effect, with a maximum IE % of 91.8% at 10⁻³ M and high corrosion inhibition stability. L4 and L6 are observed to adsorb on the CS surface, obeying the Langmuir adsorption isotherm. The L4 and L6 generate a protective organic/inorganic thin film to

inhibit surface exposure to the corrosive electrolyte. The DFT parameters and experimental findings showed good agreement. The investigated inhibitors are almost parallel to the Fe(110) surface according to MD simulation.

■ ASSOCIATED CONTENT

Supporting Information

The Supporting Information is available free of charge at <https://pubs.acs.org/doi/10.1021/acsomega.3c08282>.

Fukui indices (f_k^+ and f_k^-) of the atoms for L4 and L4H⁺ molecules and Fukui indices (f_k^+ and f_k^-) of the atoms for L6 and L6H⁺ molecules (PDF)

■ AUTHOR INFORMATION

Corresponding Authors

Fouad Benhiba – Laboratory of Advanced Materials and Process Engineering, Faculty of Sciences, Ibn Tofail University, 14000 Kenitra, Morocco; Laboratory of Materials, Nanotechnology and Environment, Faculty of Sciences, Mohammed V University in Rabat, 10500 Rabat, Morocco; Phone: 00212665201397; Email: benhibafouad@gmail.com

Abdelkader Zarrouk – Laboratory of Materials, Nanotechnology and Environment, Faculty of Sciences, Mohammed V University in Rabat, 10500 Rabat, Morocco; orcid.org/0000-0002-5495-2125; Phone: 00212665201397; Email: azarrouk@gmail.com

Authors

Loubna Adlani – Laboratory of Advanced Materials and Process Engineering, Faculty of Sciences, Ibn Tofail University, 14000 Kenitra, Morocco

Nisrine Benzbiria – Laboratory of Interface Materials Environment, Faculty of Sciences Ain Chock, Hassan II University, Mâarif B.P. 5366 Casablanca, Morocco

Abderrahim Titi – Laboratory of Applied and Environmental Chemistry (LCAE), Mohammed First University, 60000 Oujda, Morocco; Present Address: Engineering Laboratory of Organometallic, Molecular Materials and Environment (LIMOME) University Sidi Mohamed Ben Abdellah, Faculty of Sciences, Chemistry Department, P.O. Box 1796 (Atlas), 30000 Fez, Morocco

Nadia Timoudan – Laboratory of Materials, Nanotechnology and Environment, Faculty of Sciences, Mohammed V University in Rabat, 10500 Rabat, Morocco

Ismail Warad – Department of Chemistry, AN-Najah National University, 00970 Nablus, Palestine; orcid.org/0000-0001-8853-8961

Abeer AlObaid – Department of Chemistry, College of Science, King Saud University, 11451 Riyadh, Saudi Arabia

Basheer Mohammed Al-Maswari – Department of Chemistry, Yuvaraja's College, University of Mysore, Mysuru 570005 Karnataka, India; orcid.org/0000-0002-2503-208X

Rachid Touzani – Laboratory of Applied and Environmental Chemistry (LCAE), Mohammed First University, 60000 Oujda, Morocco

Hassan Zarrok – Laboratory of Advanced Materials and Process Engineering, Faculty of Sciences, Ibn Tofail University, 14000 Kenitra, Morocco

Fouad Bentiss – University Lille, CNRS, INRAE, Centrale Lille, UMR 8207, UMET-Unité Matériaux et Transformations, F-59000 Lille, France; Laboratory of Catalysis and Corrosion of Materials, Faculty of Sciences, Chouaib Doukkali University, M-24000 El Jadida, Morocco

Hassan Oudda – Laboratory of Advanced Materials and Process Engineering, Faculty of Sciences, Ibn Tofail University, 14000 Kenitra, Morocco

Complete contact information is available at:

<https://pubs.acs.org/10.1021/acsomega.3c08282>

Notes

The authors declare no competing financial interest.

ACKNOWLEDGMENTS

The authors extend their appreciation to the Researchers Supporting Project number (RSP2024R381), King Saud University, Riyadh, Saudi Arabia.

REFERENCES

- (1) Akinyemi, O. O.; Nwaokocha, C. N.; Adesanya, A. O. Evaluation of corrosion cost of crude oil processing industry. *J. Eng. Sci. Technol.* **2012**, *7* (4), 517–528.
- (2) Zhang, Z.; Ba, H.; Wu, Z.; Zhu, Y. The inhibition mechanism of maize gluten meal extract as green inhibitor for steel in concrete via experimental and theoretical elucidation. *Constr. Build. Mater.* **2019**, *198*, 288–298.
- (3) Jekayinfa, S. O.; Okekunle, P. O.; Amole, I.; Oyelade, J. A. Evaluation of corrosion cost in some selected food and agro-processing industries in Nigeria. *Anti-Corros. Methods Mater.* **2005**, *52* (4), 214–218.
- (4) Perumal, K. E. Corrosion risk analysis, risk-based inspection and a case study concerning a condensate pipeline. *Procedia Eng.* **2014**, *86*, 597–605.
- (5) Loto, R. T.; Olowoyo, O. Corrosion inhibition properties of the combined admixture of essential oil extracts on mild steel in the presence of SO_4^{2-} anions. *S. Afr. J. Chem. Eng.* **2018**, *26*, 35–41.
- (6) Dehghani, A.; Bahlakeh, G.; Ramezanzadeh, B. A detailed electrochemical/ theoretical exploration of the aqueous Chinese gooseberry fruit shell extract as a green and cheap corrosion inhibitor for mild steel in acidic solution. *J. Mol. Liq.* **2019**, *282*, 366–384.
- (7) Mohagheghi, A.; Arefinia, R. Corrosion inhibition of carbon steel by dipotassium hydrogen phosphate in alkaline solutions with low chloride contamination. *Constr. Build. Mater.* **2018**, *187*, 760–772.
- (8) Hegazy, M. A.; El-Tabei, A. S.; Bedair, A. H.; Sadeq, M. A. Synthesis and inhibitive performance of novel cationic and gemini surfactants on carbon steel corrosion in 0.5 M H_2SO_4 solution. *RSC Adv.* **2015**, *5*, 64633–64650.
- (9) Nikpour, S.; Ramezanzadeh, M.; Bahlakeh, G.; Ramezanzadeh, B.; Mahdavian, M. Eriobotrya japonica Lindl leaves extract application for effective corrosion mitigation of mild steel in HCl solution: experimental and computational studies. *Constr. Build. Mater.* **2019**, *220*, 161–176.
- (10) Ahamad, I.; Prasad, R.; Quraishi, M. A. Inhibition of mild steel corrosion in acid solution by Pheniramine drug: experimental and theoretical study. *Corros. Sci.* **2010**, *52*, 3033–3041.
- (11) Zhang, S.; Tao, Z.; Li, W.; Hou, B. The effect of some triazole derivatives as inhibitors for the corrosion of mild steel in 1M hydrochloric acid. *Appl. Surf. Sci.* **2009**, *255*, 6757–6763.
- (12) Guo, L.; Obot, I. B.; Zheng, X.; Shen, X.; Qiang, Y.; Kaya, S.; Kaya, C. Theoretical insight into an empirical rule about organic corrosion inhibitors containing nitrogen, oxygen, and sulfur atoms. *Appl. Surf. Sci.* **2017**, *406*, 301–306.
- (13) Camila, G. D.; Alexandre, G. Corrosion inhibitors—principles, mechanisms and applications. *Developments in Corrosion Protection; IntechOpen*, 2014; Vol. 16, pp 365–379.
- (14) Feng, L.; Zhang, S.; Feng, Y.; Ren, X.; Lu, H.; Tan, B.; Chen, S. Self-aggregate nanoscale copolymer of new synthesized compounds efficiently protecting copper corrosion in sulfuric acid solution. *J. Chem. Eng.* **2020**, *394*, 124909.
- (15) Mechbal, N.; Belghiti, M. E.; Benzbiria, N.; Lai, C. H.; Kaddouri, Y.; Karzazi, Y.; Touzani, R.; Zertoubi, M. Correlation between corrosion inhibition efficiency in sulfuric acid medium and the molecular structures of two newly eco-friendly pyrazole derivatives on iron oxide surface. *J. Mol. Liq.* **2021**, *331*, 115656.
- (16) Winkler, D. Predicting the performance of organic corrosion inhibitors. *Metals* **2017**, *7* (12), 553.
- (17) Benzbiria, N.; Thoume, A.; Echihi, S.; Belghiti, M. E.; Elmakssoudi, A.; Zarrouk, A.; Azzi, M.; Zertoubi, M. Coupling of experimental and theoretical studies to apprehend the action of benzodiazepine derivative as a corrosion inhibitor of carbon steel in 1M HCl. *J. Mol. Struct.* **2023**, *1281*, 135139.
- (18) Zhang, W.; Ma, R.; Liu, H.; Liu, Y.; Li, S.; Niu, L. Electrochemical and surface analysis studies of 2-(quinolin-2-yl)-quinazolin-4(3H)-one as corrosion inhibitor for Q235 steel in hydrochloric acid. *J. Mol. Liq.* **2016**, *222*, 671–679.
- (19) Belayachi, M.; Serrar, H.; Zarrok, H.; El Assry, A.; Zarrouk, A.; Oudda, H.; Boukhris, S.; Hammouti, B.; Ebenso, E. E.; Geunbour, A. New pyrimidothiazine Derivative as Corrosion Inhibitor for Carbon Steel in Acidic Media. *Int. J. Electrochem. Sci.* **2015**, *10*, 3010–3025.
- (20) Tayebi, H.; Bourazmi, H.; Himmi, B.; El Assry, A.; Ramli, Y.; Zarrouk, A.; Geunbour, A.; Hammouti, B.; Ebenso, E. E. An electrochemical and theoretical evaluation of new quinoline derivative

as a corrosion inhibitor for carbon steel in HCl solutions. *Der Pharm. Lett.* **2014**, *6* (6), 20–34.

(21) Bendaha, H.; Zarrouk, A.; Aouniti, A.; Hammouti, B.; El Kadiri, S.; Salghi, R.; Touzani, R. Adsorption and corrosion inhibitive properties of some tripodal pyrazolic compounds on mild steel in hydrochloric acid systems. *Phys. Chem. News* **2012**, *64*, 95–103.

(22) Zarrok, H.; Salghi, R.; Zarrouk, A.; Hammouti, B.; Oudda, H.; Bazzi, Lh.; Bammou, L.; Al-Deyab, S. S. Investigation of the Inhibition Effect of N-1-Naphthylethylenediamine Dihydrochloride Monomethanolate on the C38 Steel Corrosion in 0.5M H₂SO₄. *Der Pharm. Chem.* **2012**, *4* (1), 407–416.

(23) Zarrok, H.; Saddik, R.; Oudda, H.; Hammouti, B.; El Midaoui, A.; Zarrouk, A.; Benchat, N.; Ebn Touhami, M. 5-(2-Chlorobenzyl)-2,6-Dimethylpyridazin-3-One: An efficient Inhibitor of C38 Steel Corrosion in Hydrochloric Acid. *Der Pharm. Chem.* **2011**, *3* (5), 272–282.

(24) Zhou, Y.; Xu, S.; Guo, L.; Zhang, S.; Lu, H.; Gong, Y.; Gao, F. Evaluating two new Schiff bases synthesized on the inhibition of corrosion of copper in NaCl solutions. *RSC Adv.* **2015**, *5*, 14804–14813.

(25) Benzbiria, N.; Echihi, S.; Belghiti, M. E.; Thoume, A.; Elmakssoudi, A.; Zarrouk, A.; Zertoubi, M.; Azzi, M. Novel synthesized benzodiazepine as efficient corrosion inhibitor for copper in 3.5% NaCl solution. *Mater. Today: Proc.* **2021**, *37*, 3932–3939.

(26) Frontini, M. A.; Schreiner, W. W.; Vázquez, M.; Valcarce, M. B. Nitrite corrosion inhibition in chloride-rich electrolytes correlated to the electrical properties of surface films on carbon steel. *Constr. Build. Mater.* **2019**, *227*, 116650.

(27) Laadam, G.; Benhiba, F.; El Faydy, M.; Titi, A.; Al-Gorair, A. S.; Alshareef, M.; Hawsawi, H.; Touzani, R.; Warad, I.; Bellaouchou, A.; et al. Anti-corrosion performance of novel pyrazole derivative for carbon steel corrosion in 1 M HCl: Computational and experimental studies. *Inorg. Chem. Commun.* **2022**, *145*, 109963.

(28) Jasim, A. S.; Rashid, K. H.; AL-Azawi, K. F.; Khadom, A. A. Synthesis of a novel pyrazole heterocyclic derivative as corrosion inhibitor for low-carbon steel in 1M HCl: Characterization, gravimetric, electrochemical, mathematical, and quantum chemical investigations. *Results Eng.* **2022**, *15*, 100573.

(29) Laadam, G.; El Faydy, M.; Benhiba, F.; Titi, A.; Amegroud, H.; Al-Gorair, A. S.; Hawsawi, H.; Touzani, R.; Warad, I.; Bellaouchou, A.; et al. Outstanding anti-corrosion performance of two pyrazole derivatives on carbon steel in acidic medium: Experimental and quantum-chemical examinations. *J. Mol. Liq.* **2023**, *375*, 121268.

(30) Thoume, A.; Benhiba, F.; Elmakssoudi, A.; Left, D. B.; Benzbiria, N.; Warad, I.; Dakir, M.; Azzi, M.; Zertoubi, M.; Zarrouk, A. Corrosion inhibition behavior of chalcone oxime derivatives on carbon steel in 0.5 M H₂SO₄. *J. Appl. Electrochem.* **2021**, *51*, 1755–1770.

(31) Shaban, M. M.; El Basiony, N. M.; Radwan, A. B.; El-Katori, E. E.; Abu-Rayyan, A.; Bahtiti, N. H.; Abdou, M. M. Electrochemical Investigation of C-Steel Corrosion Inhibition, In Silico, and Sulfate-Reducing Bacteria Investigations Using Pyrazole Derivatives. *ACS Omega* **2023**, *8* (33), 30068–30080.

(32) Al Garadi, W.; Jrajri, K.; El Faydy, M.; Benhiba, F.; El Ghayati, L.; Sebbar, N. K.; Essassi, E. M.; Warad, I.; Guenbour, A.; Bellaouchou, A.; Jama, C.; Alsalme, A.; Zarrouk, A. 4-phenyl-decahydro-1H-1,5-benzodiazepin-2-one as novel and effective corrosion inhibitor for carbon steel in 1 M HCl solution: A combined experimental and empirical studies. *J. Indian Chem. Soc.* **2022**, *99* (11), 100742.

(33) Wen, J.; Zhang, X.; Chen, J.; Liu, T.; Zhou, Y.; Li, L. Synthesis of 1, 4, 7-triazaheptane derivative and its corrosion inhibition for mild steel in the hydrochloric medium. *J. Ind. Eng. Chem.* **2022**, *107*, 333–345.

(34) Benzbiria, N.; Thoume, A.; Ait El Caid, Z.; Echihi, S.; Elmakssoudi, A.; Zarrouk, A.; Zertoubi, M. An investigation on the utilization of a synthesized benzodiazepine derivative as a corrosion inhibitor for carbon steel in sulfuric solution: Chemical and

electrochemical synthesis, surface analysis (SEM/AFM), DFT and MC simulation. *Colloids Surf., A* **2024**, *681*, 132744.

(35) Akroujai, E. H.; Chetioui, S.; Benzbiria, N.; Barrahi, A.; Chakra, A.; Djedouani, A.; Chtita, S.; Lazar, S.; Warad, I.; Bellaouchou, A.; Assouag, M.; Zarrouk, A. ((E)-1-((4-Fluorophenyl)diazanyl)-naphthalen-2-ol as an innovative and efficient corrosion inhibitor for carbon steel in 1 M HCl solution: Electrochemical analysis coupled with electronic/atomicscale computational simulations. *Int. J. Corros. Scale Inhib.* **2023**, *12* (3), 1102–1135.

(36) Abd El-Lateef, H. M.; Abo-Riya, M. A.; Tantawy, A. H. Empirical and quantum chemical studies on the corrosion inhibition performance of some novel synthesized cationic Gemini surfactants on carbon steel pipelines in acid pickling processes. *Corros. Sci.* **2016**, *108*, 94–110.

(37) Laabaissi, T.; Benhiba, F.; Rouifi, Z.; Missioui, M.; Ourrak, K.; Oudda, H.; Ramlı, Y.; Warad, I.; Allali, M.; Zarrouk, A. New quinoxaline derivative as a green corrosion inhibitor for mild steel in mild acidic medium: Electrochemical and theoretical studies. *Int. J. Corros. Scale Inhib.* **2019**, *8* (2), 241–256.

(38) Kharbach, Y.; Qachchachi, F. Z.; Haoudi, A.; Tourabi, M.; Zarrouk, A.; Jama, C.; Olasunkanmi, L. O.; Ebenso, E. E.; Bentiss, F. Anticorrosion performance of three newly synthesized isatin derivatives on carbon steel in hydrochloric acid pickling environment: Electrochemical, surface and theoretical studies. *J. Mol. Liq.* **2017**, *246*, 302–316.

(39) Fergachi, O.; Benhiba, F.; Rbaa, M.; Touri, R.; Ouakki, M.; Galai, M.; Lakhri, B.; Oudda, H.; Touhami, M. E. Experimental and Theoretical Study of Corrosion Inhibition of Mild Steel in 1.0 M HCl Medium by 2-(4-(chlorophenyl)-1H-benzimidazole-1-yl)-phenylmethanone. *Mater. Res.* **2018**, *21* (6), 1–11.

(40) Oubaaqa, M.; Ouakki, M.; Rbaa, M.; Abousalem, A. S.; Maatallah, M.; Benhiba, F.; Jarid, A.; Ebn Touhami, M.; Zarrouk, A. Insight into the corrosion inhibition of new amino-acids as efficient inhibitors for mild steel in HCl solution: Experimental studies and theoretical calculations. *J. Mol. Liq.* **2021**, *334*, 116520.

(41) Andersen, H. C. Molecular dynamics simulations at constant pressure and/or temperature. *J. Chem. Phys.* **1980**, *72*, 2384–2393.

(42) Geler, E.; Azambuja, D. Corrosion inhibition of copper in chloride solutions by pyrazole. *Corros. Sci.* **2000**, *42* (4), 631–643.

(43) Goyal, M.; Vashisht, H.; Kumar, A.; Kumar, S.; Bahadur, I.; Benhiba, F.; Zarrouk, A. Iso pentyl triphenyl phosphonium bromide ionic liquid as a newly effective corrosion inhibitor on metal-electrolyte interface in acidic medium: Experimental, surface morphological (SEM-EDX & AFM) and computational analysis. *J. Mol. Liq.* **2020**, *316*, 113838.

(44) Thoume, A.; Benmessaoud Left, D.; El Makssoudi, A.; Benhiba, F.; Zarrouk, A.; Benzbiria, N.; Warad, I.; Dakir, M.; Azzi, M.; Zertoubi, M. Chalcone oxime derivatives as new inhibitors corrosion of carbon steel in 1 M HCl solution. *J. Mol. Liq.* **2021**, *337* (2), 116398.

(45) Shaban, S. M.; Aiad, I.; El-Sukkary, M. M.; Soliman, E. A.; El-Awady, M. Y. Inhibition of mild steel corrosion in acidic medium by vanillin cationic surfactants. *J. Mol. Liq.* **2015**, *203*, 20–28.

(46) Kumar, R.; Yadav, O. S.; Singh, G. Electrochemical and surface characterization of a new ecofriendly corrosion inhibitor for mild steel in acidic media: a cumulative study. *J. Mol. Liq.* **2017**, *237*, 413–427.

(47) Benhiba, F.; Hsissou, R.; Benzekri, Z.; Echihi, S.; El-Bilal, J.; Boukhris, S.; Bellaouchou, A.; Guenbour, A.; Oudda, H.; Warad, I.; Sebbar, N. K.; Zarrouk, A. DFT/electronic scale, MD simulation and evaluation of 6-methyl-2-(p-tolyl)-1,4-dihydroquinoxaline as a potential corrosion inhibitor. *J. Mol. Liq.* **2021**, *335*, 116539.

(48) Zarrouk, A.; Hammouti, B.; Zarrok, H.; Al-Deyab, S. S.; Messali, M. Temperature effect, activation energies and thermodynamic adsorption studies of Lcysteine methyl ester hydrochloride as copper corrosion inhibitor in nitric acid 2M. *Int. J. Electrochem. Sci.* **2011**, *6*, 6261–6274.

(49) El Faydy, M.; Benhiba, F.; About, H.; Kerroum, Y.; Guenbour, A.; Lakhri, B.; Warad, I.; Verma, C.; Sherif, E.-S. M.; Ebenso, E. E.; et al. Experimental and computational investigations on the anti-

- corrosive and adsorption behavior of 7-N,N'-dialkylaminomethyl-8-Hydroxyquinolines on C40E steel surface in acidic medium. *J. Colloid Interface Sci.* **2020**, *576*, 330–344.
- (50) Yildiz, R. Adsorption and inhibition effect of 2,4-diamino-6-hydroxypyrimidine for mild steel corrosion in HCl medium: experimental and theoretical investigation. *Ionics* **2019**, *25*, 859–870.
- (51) Riggs, O. L. *Corrosion Inhibitors*, 2nd ed.; Nathan, C.C.; National Association of Corrosion Engineers: Houston, TX, 1973.
- (52) Benhiba, F.; Missiou, M.; Lamghafri, S.; Hsissou, R.; Bellaouchou, A.; Oudda, H.; Lamhamdi, A.; Warad, I.; Raml, Y.; Zarrouk, A. Theoretical and Experimental Studies of 1-Dodecyl-3-phenylquinoxalin-2(1H)-one as a Sustainable Corrosion Inhibitor for Carbon Steel in Acidic Electrolyte. *Coatings* **2023**, *13*, 1109.
- (53) El yaktini, A.; Lachiri, A.; El Faydy, M.; Benhiba, F.; Zarrok, H.; El Azzouzi, M.; Zertoubi, M.; Azzi, M.; Lakhrissi, B.; Zarrouk, A. Practical and Theoretical Study on the Inhibitory Influences of New Azomethine Derivatives Containing an 8-Hydroxyquinoline Moiety for the Corrosion of Carbon Steel in 1 M HCl. *Orient. J. Chem.* **2018**, *34* (6), 3016–3029.
- (54) Torres, V. V.; Amado, R. S.; de Sá, C. F.; Fernandez, T. L.; Riehl, C. A. d. S.; Torres, A. G.; D'Elia, E. Inhibitory action of aqueous coffee ground extracts on the corrosion of carbon steel in HCl solution. *Corros. Sci.* **2011**, *53*, 2385–2392.
- (55) Liu, Y. W.; Chen, Y.; Chen, X. H.; Yang, Z. N.; Xie, Y.; Zhang, Z. Study on adsorption behavior of ketoconazole on Q235 mild steel in 1.0 M HCl solution with electrochemical measurement. *J. Alloys Compd.* **2018**, *758*, 184–193.
- (56) Ouici, H. B.; Benali, O.; Harek, Y.; Al-Deyab, S. S.; Larabi, L.; Hammouti, B. Influence of the 2-Mercapto-1-Methyl Imidazole (MMI) on the Corrosion Inhibition of Mild Steel in 5% HCl. *J. Electrochem. Sci.* **2012**, *7*, 2304–2319.
- (57) Boudjellal, F.; Ouici, H. B.; Guendouzi, A.; Benali, O.; Sehmi, A. Experimental and theoretical approach to the corrosion inhibition of mild steel in acid medium by a newly synthesized pyrazole carbothioamide heterocycle. *J. Mol. Struct.* **2020**, *1199*, 127051.
- (58) Attou, A.; Tourabi, M.; Benikdes, A.; Benali, O.; Ouici, H. B.; Benhiba, F.; Zarrouk, A.; Jama, C.; Bentiss, F. Experimental studies and computational exploration on the 2-amino-5-(2-methoxyphenyl)-1,3,4-thiadiazole as novel corrosion inhibitor for mild steel in acidic environment. *Colloids Surf., A* **2020**, *604*, 125320.
- (59) MacDonald, D. D. Review of mechanistic analysis by electrochemical impedance spectroscopy. *Electrochemical and Optical Techniques for the Study and Monitoring of Metallic Corrosion*; Ferreira, M. G. S., Melendres, C. A., Eds.; NATO ASI Series (Series E: Applied Sciences); Springer: Dordrecht, 1991; Vol. 203, pp 31–68.
- (60) Abd Allah, M.; Hegazy, M. A.; Ahmed, H.; Al-Gorair, A. S.; Hawsawi, H.; Morad, M.; Benhiba, F.; Warad, I.; Zarrouk, A. Appraisal of synthetic cationic Gemini surfactants as highly efficient inhibitors for carbon steel in the acidization of oil and gas wells: An experimental and computational approach. *RSC Adv.* **2022**, *12*, 17050–17064.
- (61) Benhiba, F.; Hsissou, R.; Benzekri, Z.; Echih, S.; El-Blilak, J.; Boukhris, S.; Bellaouchou, A.; Guenbour, A.; Oudda, H.; Warad, I.; Sebbar, N. K.; Zarrouk, A. DFT/electronic scale, MD simulation and evaluation of 6-methyl-2-(p-tolyl)-1,4-dihydroquinoxaline as a potential corrosion inhibition. *J. Mol. Liq.* **2021**, *335*, 116539.
- (62) El Faydy, M.; Benhiba, F.; Lakhrissi, B.; Touhami, M. E.; Warad, I.; Bentiss, F.; Zarrouk, A. The inhibitive impact of both kinds of 5-isothiocyanatomethyl-8-hydroxyquinoline derivatives on the corrosion of carbon steel in acidic electrolyte. *J. Mol. Liq.* **2019**, *295*, 111629.
- (63) El Faydy, M.; Lakhrissi, B.; Jama, C.; Zarrouk, A.; Olasunkanmi, L. O.; Ebenso, E. E.; Bentiss, F. Electrochemical, surface and computational studies on the inhibition performance of some newly synthesized 8-hydroxyquinoline derivatives containing benzimidazole moiety against the corrosion of carbon steel in phosphoric acid environment. *J. Mater. Res. Technol.* **2020**, *9* (1), 727–748.
- (64) Rbaa, M.; Fardioui, M.; Verma, C.; Abousalem, A. S.; Galai, M.; Ebenso, E. E.; Guedira, T.; Lakhrissi, B.; Warad, I.; Zarrouk, A. 8-Hydroxyquinoline based chitosan derived carbohydrate polymer as biodegradable and sustainable acid corrosion inhibitor for mild steel: experimental and computational analyses. *Int. J. Biol. Macromol.* **2020**, *155*, 645–655.
- (65) Cao, S.; Liu, D.; Zhang, P.; Yang, L.; Yang, P.; Lu, H.; Gui, J. Green Bronsted acid ionic liquids as novel corrosion inhibitors for carbon steel in acidic medium. *Sci. Rep.* **2017**, *7*, 8773.
- (66) Becke, A. Density-functional thermochemistry. III. The role of exact exchange. *J. Chem. Phys.* **1993**, *98*, 5648–5652.
- (67) Tomasi, J.; Mennucci, B.; Cammi, R. Quantum mechanical continuum solvation models. *Chem. Rev.* **2005**, *105* (8), 2999–3094.
- (68) MarvinSketch. *MarvinSketch Software*, Version: 18.22; Chem-Axon Ltd., 2018.
- (69) El yaktini, A.; Lachiri, A.; El Faydy, M.; Benhiba, F.; Zarrok, H.; El Azzouzi, M.; Zertoubi, M.; Azzi, M.; Lakhrissi, B.; Zarrouk, A. Inhibitor effect of new azomethine derivative containing an 8-hydroxyquinoline moiety on corrosion behavior of mild carbon steel in acidic media. *Int. J. Corros. Scale Inhib.* **2018**, *7* (4), 609–632.
- (70) Benhiba, F.; Sebbar, N. K.; Bourazmi, H.; Belghiti, M. E.; Hsissou, R.; Hökelek, T.; Bellaouchou, A.; Guenbour, A.; Warad, I.; Oudda, H.; Zarrouk, A.; Essassi, E. M. Corrosion inhibition performance of 4-(prop-2-ynyl)-[1,4]-benzothiazin-3-one against mild steel in 1M HCl solution: Experimental and theoretical studies. *Int. J. Hydrogen Energy* **2021**, *46* (51), 25800–25818.
- (71) Hamed, R.; Jodeh, S.; Hanbali, G.; Safi, Z.; Berisha, A.; xhaxhiu, K.; Dagdag, O. Eco-Friendly Synthesis and Characterization of Double-Crossed Link 3D Graphene Oxide Functionalized With Chitosan for Adsorption of Sulfamethazine From Aqueous Solution: Experimental and DFT Calculations. *Front. Environ. Sci.* **2022**, *10*, 930693.
- (72) Benhiba, F.; Hsissou, R.; Abderrahim, K.; Serrar, H.; Rouifi, Z.; Boukhris, S.; Kaichouh, G.; Bellaouchou, A.; Guenbour, A.; Oudda, H.; Warad, I.; Zarrouk, A. Development of New Pyrimidine Derivative Inhibitor for Mild Steel Corrosion in Acid Medium. *J. Bio-Tribo-Corros.* **2022**, *8* (2), 36.
- (73) Alibakhshi, E.; Ramezanzadeh, M.; Bahlakeh, G.; Ramezanzadeh, B.; Mahdavian, M.; Motamedi, M. Glycyrrhiza glabra leaves extract as a green corrosion inhibitor for mild steel in 1 M hydrochloric acid solution: experimental, molecular dynamics, Monte Carlo and quantum mechanics study. *J. Mol. Liq.* **2018**, *255*, 185–198.
- (74) Faydy, M. E.; Benhiba, F.; Warad, I.; Saoiabi, S.; Alharbi, A.; Alluhaybi, A. A.; Lakhrissi, B.; Abdallah, M.; Zarrouk, A. Bisquinolineanalogs as corrosion inhibitors for carbon steel in acidic electrolyte: Experimental, DFT, and molecular dynamics simulation approaches. *J. Mol. Struct.* **2022**, *1265* (1–2), 133389.
- (75) Abouchane, M.; Dkhireche, N.; Rbaa, M.; Benhiba, F.; Ouakki, M.; Galai, M.; Lakhrissi, B.; Zarrouk, A.; Ebn Touhami, M. Insight into the corrosion inhibition performance of two quinoline-3-carboxylate derivatives as highly efficient inhibitors for mild steel in acidic medium: Experimental and theoretical evaluations. *J. Mol. Liq.* **2022**, *360*, 119470.
- (76) Berrissoul, A.; Ouarhach, A.; Benhiba, F.; Romane, A.; Guenbour, A.; Outada, H.; Dafali, A.; Zarrouk, A. Exploitation of a new green inhibitor against mild steel corrosion in HCl: Experimental, DFT and MD simulation approach. *J. Mol. Liq.* **2022**, *349*, 118102.